Biological Scaffolds for the Peptide-Directed Assembly of Nanoscale Materials and Devices

by

Daniel Joseph Solis

B.S. Chemistry
B.A. Physics

California Polytechnic State University, San Luis Obispo, CA 93407.
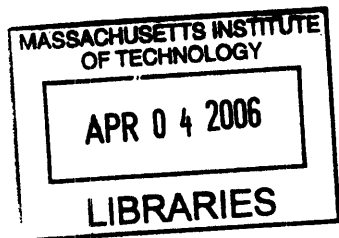
2001

SUBMITTED TO THE DEPARTMENT OF CHEMISTRY IN PARTIAL FULFILMENT OF
THE REQUIREMENTS FOR THE DEGREE OF

DOCTORATE OF PHILOSOPHY IN PHYSICAL CHEMISTRY
AT THE
MASSACHUSETTS INSTITUTE OF TECHNOLOGY, CAMBRIDGE, MA 02139

ARCHIVES February 2006.

© 2006 Daniel J. Solis
All rights reserved.

The author hereby grants to MIT permission to reproduce and to distribute publicly paper and
electronic copies of this thesis document in whole or part in any medium now known
or hereafter created.

Signature of Author

Daniel J. Solis
November 10th, 2005

Certified by

Angela M. Belcher
Professor of Materials Science & Engineering
Thesis Supervisor

Accepted by

Robert W. Field
Chairman, Departmental Committee on Graduate Students
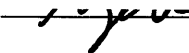
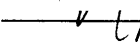THESIS COMMITTEE CERTIFICATION OF APPROVAL

OF

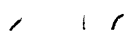# Biological Scaffolds for the Peptide-Directed Assembly of Nanoscale Materials and Devices

by

Daniel Joseph Solis

GRADUATE THESIS COMMITTEE

Angela M. Belcher
Professor of Materials Science
& Bioengineering

Moungi G. Bawendi
Professor of Chemistry
Thesis Committee Chair

Keith A. Nelson
Professor of Chemistry

Biological Scaffolds for the Peptide-Directed Assembly of Nanoscale Materials and Devices

by

Daniel Joseph Solis

Submitted to the Department of Chemistry on February 1, 2006,
in partial fulfillment of the requirements for the
Degree of Doctorate of Philosophy in Physical Chemistry.

Abstract

The utilization of biological factors in the design, synthesis and fabrication of nano-scaled materials and devices presents novel, large scale solutions for the realization of future technologies. In particular, we have genetically modified the M13 Filamentous Bacteriophage for its use as a biological scaffold in the peptide-controlled nucleation and patterning of nanoscale semiconducting and magnetic materials. Through evolutionary phage display screening of inorganic substrates, functional peptides that influence material properties such as size, phase and composition during nucleation have been identified. The incorporation of these specific, nucleating peptides into the generic scaffold of the M13 coat structure provides a viable linear template for the directed synthesis of semiconducting and magnetic nanowires. Through further modification of the remaining proteins on the virus scaffold, other functionalities can be incorporated such as the directed patterning of the virus/nanowires assemblies into nanoscaled devices with tunable properties as determined by the genetic information carried within the virus scaffold. Multi-functional viruses provide a truly self assembled system for the design and execution of a myriad of nanoscaled devices in a green, scalable and cost effective manner.

Thesis Supervisor : Angela M. Belcher
Title : John Chipman Professor of Materials Science & Engineering and Biological Engineering.

ACKNOWLEDGEMENTS

TABLE OF CONTENTS

LIST OF TABLES

LIST OF FIGURES

1.0 *Introduction*

The reliance of future technologies on developing scalable and economic methods for the fabrication of one-dimensional systems has spurred intense and rapid progress in the interdisciplinary field of materials science. In particular, one-dimensional materials have been enthusiastically pursued for their applications in the study of electrical transport (*1*), optical phenomena (*2*), and as functional units in nanoscaled circuitry (*3*). Pursuit of "bottom up" methods for the synthesis of semiconducting, metallic and magnetic nanowires has yielded strategies including, but not limited to, vapor liquid solid (VLS) (*4*), chemical (*5*), solvothermal, vapor phase, and template-directed fabrication (*6*). Although each method developed for the production of nanowires has had success in achieving high quality materials, no distinct strategy to date has yielded monodisperse, crystalline nanowires of radically different compositions. The realization of such a system would require the combination of substrate specific ligands with the predictability of self-assembly commonly found in nature. Recently, biological factors have been exploited as synthesis directors for nanofibers (*7, 8*), virus-based particle cages (*9*), virus-particle assemblies (*10, 11*), and non-specific peptide templates (*12*). This is due to the high degree of organization, ease of chemical modification and naturally occurring self-assembly motifs inherent in these systems.

The development of the virus based scaffold for synthesizing and assembling nanoscale materials into function architectures is presented (figure 1.1). The ability to store information about a material, including composition, phase, and crystallographic detail, within the genetic code of the M13 bacteriophage virus DNA has proven to be a viable means of synthesizing and organizing materials on the nanometer scale (*13,14*). The use of phage display techniques

(utilizing peptide libraries consisting of $\sim 10^9$ random sequences) has led to the discovery of material specific peptides having preferential binding (*13*), control over nanoparticle nucleation (*14*), and the ability to order based on the inherent shape anisotropy of the filamentous M13 virus (*11*).
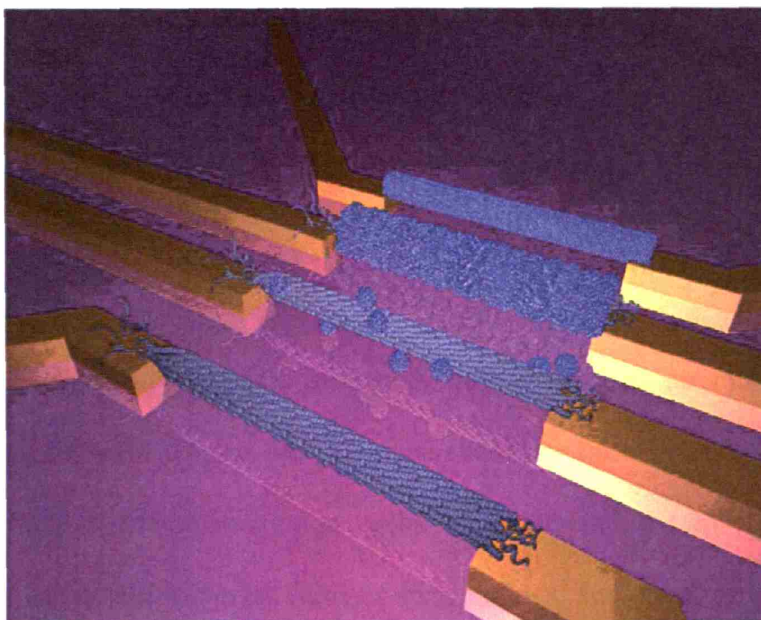
Figure 1.1 Proposed device assembly using a substrate binding peptide on the proximal tip of the virus to anchor it specifically to pre-patterned gold electrodes. Peptides expressed along the length of the phage can then induce nucleation of technologically relevant materials between the electrode gap. Thermal removal of the organic template results in continuous inorganic nanowires connected to the electrodes creating a functional device.

Because the protein sequences responsible for these attributes are gene linked and contained within the capsid of the virus, exact genetic copies of the virus scaffold are easily reproduced by infection into its bacterial host. The exploitation of the self-assembly motifs employed by the M13 bacteriophage to produce a biological scaffold provides a means of generating a complex, highly ordered, and economical template for the general synthesis of single crystal nanowires. By introducing programmable genetic control over the composition, phase and assembly of nanoparticles, a generic template for the universal synthesis of a variety of materials can be realized. Further advances in the fabrication of nanoscale materials and

devices can be achieved through modification of the remaining four proteins in the virus to incorporate device-assembly directors. Overall, modification of biological systems by the introduction of substrate specific peptides presents a means of achieving well ordered nanomaterials in a cost-effective and scalable manner (*15*). The following chapters will discuss the selection of functional peptides exhibiting a binding affinity for specific materials, the genetic manipulation of these functional peptides into different areas of the M13 bacteriophage scaffold, and the subsequent ability to control materials synthesis and assembly.

1.1 *Biomineralization*

Nature's ability to form inorganic structures with controlled structure and properties, developed over millions of years, provides a unique chemistry for developing inorganic-organic materials. The field of biomineralization seeks to understand the mechanisms by which biological systems can uptake elements from its surroundings, and organize them into complex, highly ordered structures of defined functionality (*16*). There are many types of organisms that utilize biomineralization, ranging from single-celled coccolithophorids (figure 1.2) that assemble calcite cages to mammals who depend on the biologically controlled mineralization of hydroxyapetite for bones.
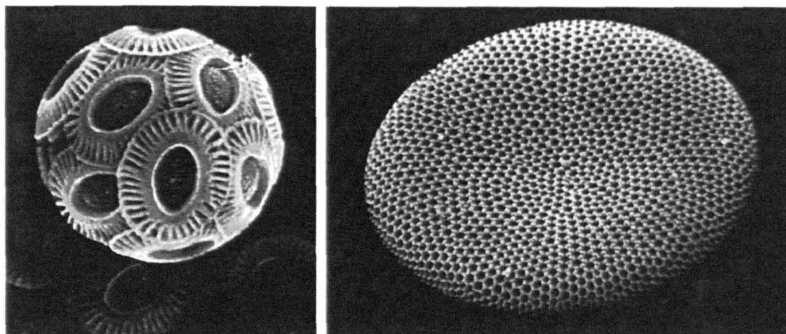
Although these materials provide essential life functions for many organisms (*17*), it is their unique physical properties and inherently green synthesis of materials with precise control that has garnered attention from the materials community as a facile route to nanoscaled components for next generation technologies. Biomineralized materials are ordered over multiple length scales (*18*) beginning at the atomistic level with control over crystallographic phase and orientation and composition, to nanoscaled building blocks of controlled shape and size, to organized micro and macroscopic heterostructures(*19*). The materials also exhibit desirable material characteristics such as fracture toughness, self-correction or "healing" and single crystal growth. Furthermore, biomineralization reactions proceed under aqueous conditions at or below ambient temperatures, yet often produce polymorphs typically synthesized at elevated temperatures and pressures. As an example, the shell of the red abalone (*haliotis rufescens*) has a "brick and mortar" like construction of aragonite tablets (a metastable phase of calcium carbonate) separated by layers of acidic glycoprotein's (figure 1.3), which gives the shell a fracture resistance 3000 times greater than geological aragonite (*20*).
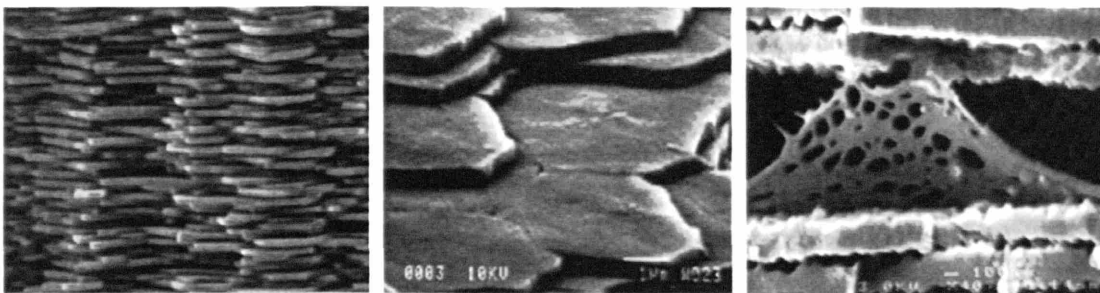
Figure 1.3 Scanning Electron Micrographs of the nacre component of the *haliotis rufescens* shell. The brick and mortar structure is evident and exhibits long range ordering.

Other examples of biomineralization systems include magnetotactic bacteria that produce 35-120nm diameter, single-domain, ferromagnetic Fe_3O_4 particles, allowing for the bacteria to migrate along the earth's magnetic field (*21*). Another common biomineralization product is marine silica (SiO_2) as found in diatoms and sea sponge spicules. The successful isolation of biomineralization proteins, and their ability to maintain functionality in vitro, has provided many successes in understanding the mechanisms behind biomineralization. However, the complexity of natural systems has impeded the complete understanding of the biomineralization process, which had hindered the progress in extending the classes of materials that can be processed by this chemistry. In order to exploit the tremendous advantages of biomineralization, a rapid method for developing functional, material-specific peptides needed to be developed in order to extend the materials available from common minerals, to technologically relevant materials including semiconductors, conductors, and highly anisotropic magnetic materials.

1.2 *Phage Display*

Almost all biological processes in living organisms rely on specific, protein-ligand interactions. Biomineralization is no different in that the inorganic substrate serves as the ligand, and a highly specific biomolecule dictates the organization and construction of the inorganic structure. There are two common techniques for isolating biomolecules that exhibit the necessary affinity for specific targets, both routinely used in the pharmaceutical industry, Rational design and Combinatorial screening. Both of these provide pathways for developing new biomineralization chemistries for synthesizing materials not found in nature. However, because the exact mechanisms for biomineralization are still not fully understood, and the complexity of biological systems, there is usually poor correlation between computer predictions

of biomolecule functionality and that observed in vitro. Also, the computational costs of analyzing the vast number of relevant mutants precludes this method from being a practical and rapid method for developing bioinorganic synthesis routes for the multiple classes of materials needed to produce the complex architectures found in today's technology. The second approach of using a combinatorial library to screen a target provides a rapid and economical means of identifying biomolecules that exhibit the required specificity for a given target, in this case an inorganic substrate. Combinatorial libraries comprised of biological systems can also employ the same evolutionary processes found in nature of mutation and selection. The main limitation of combinatorial libraries then lies in their low complexity and sample size. There are multiple types of libraries available including combinatorial chemistry, yeast two way systems, ribosomal display and cell surface display however, phage display was chosen for its combinatorial size, the complexity of its banks, the diversity of applications, and its ease of use.

Phage display libraries are systems in which a peptide or protein is expressed (displayed) on the surface of a filamentous bacteriophage virus (*22*). These libraries are commercially available with 10^9 molecules, but have been synthesized with banks as high as 10^{12} (*23*). In essence, phage display is performed by incubating the target substrate with the phage library, followed by washing of the unbound phage and elution of the specifically bound phage. The eluted phage are then amplified, creating an enriched pool for subsequent screenings. The affinity of the selected phage for the target can be tailored either through employing more stringent washings, method of elution, or by the desired binding constants as determined via kinetic screening of substrates (figure 1.4).
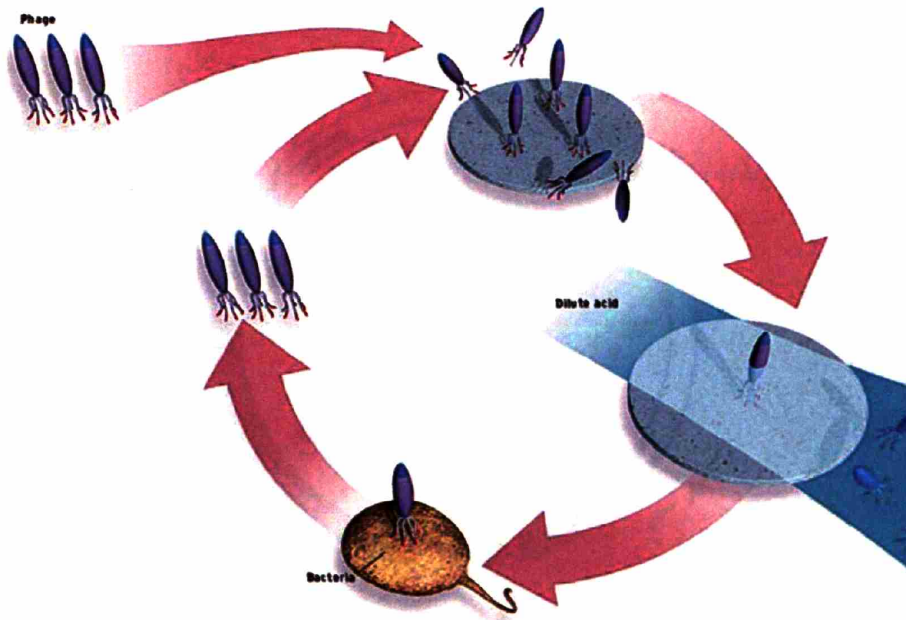
Figure 1.4 Introduction of the library (top left) to the substrate, is followed by washing and acid elution of the bound phage. Bacterial amplification enriches the phage pool, which is then screened against the same target. This process is repeated until a dominant binding sequence can be determined. (image from IEEE spectrum, Germs that build circuits, online.)

1.3 *M13 Bacteriophage*

The M13 class of bacteriophage, used in this work, is approximately 880nm long by 6nm wide, and is comprised of five capsid proteins that encapsulate a single stranded DNA. The M13 phage DNA has 9 genes that encode for 11 proteins grouped on the single stranded, covalently closed DNA in order of their functionality during the life cycle of the virus (*24*). They are classified into DNA replication proteins (gene products (gP) II,V,X), Capsid proteins (gP III, VI, VII, VIII, IX) and assembly proteins (gP I, IV, XI). The wild type (or naturally occurring, unmodified M13 phage) genome is given in figure 1.5. Addition of a randomized peptide insert on the gene III and a gene giving antibiotic resistance is added to the genome to create the gPIII library (*25*).
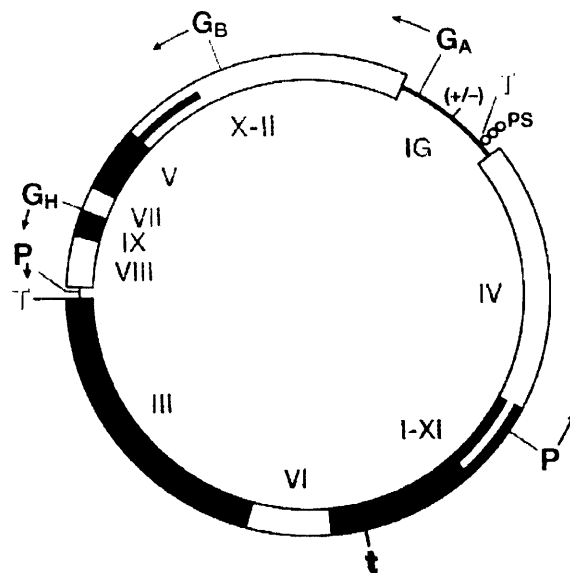
Figure 1.5 The wild type genome of the Ff class of filamentous bacteriophage, which includes the M13 phage.

The five capsid proteins create a vesicle for DNA delivery and is comprised of: approximately five copies of the gPIII and gPVI as a complex at the proximal tip of the bacteriophage (as it is the first part of the virus to enter the bacterial host, and the first to exit); approximately five copies of a similar complex of the gP VII and IX and the distal tip of the bacteriophage; and ~ 2700 copies of the gPVIII in the form of an uninterrupted alpha helix, in an overlapping shingle-type array having a five fold symmetry rotational axis with a twofold screw axis pitch of 3.2nm (figure 1.6). The pVIII monomer is then tilted with respect to the c-axis of the virus, allowing for it to wrap around the axis of the virus with a right handed twist (26). By incorporating standard combinatorial genetics to the M13 bacteriophage, chimeric proteins can be synthesized and incorporated into the phage during assembly. There seems to be no limit as to the size and type of peptide or protein that can be fused to the gPIII (27), however a limit of approximately six amino acids is imposed of fusions to the gPVIII (28). Peptides larger than six amino acids, or that are sterically bulky, and have large overall charge have deleterious effects on phage

assembly and will not be present in the final phage assembly (there are of course exceptions to this, but they require specialized DNA vectors, *29.*)
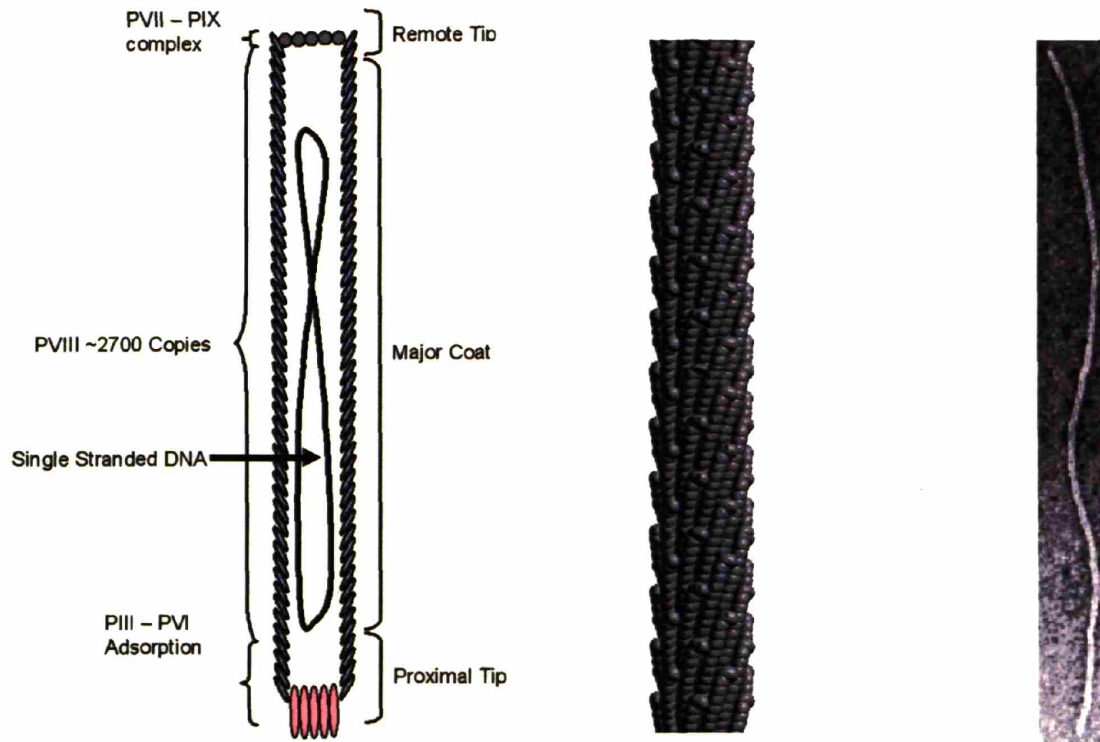
Figure 1.6. A diagram of the M13 bacteriophage showing the location of the 5 capsid proteins with respect to the single stranded DNA (left.) Recreation of the virus capsid from fiber x-ray studies as given in the pdb file # 1ifj (center.) Transmission Electron micrograph of a negatively stained wild type M13 bacteriophage (stained with uranyl acetate.) the virus is approximately 880nm long and 6nm wide (right.)

The ability to genetically modify the M13 bateriophage has increased the usability of these libraries through incorporation of antibiotic resistance to reduce contamination and through the implementation of the tittering method as a reliable assay for quantifying the number of phage present in a system and as a simple means of harvesting single phage for DNA sequencing.

Tittering exploits the *lacZ* gene that has been incorporated into the genome of the library phage. After infection of the phage into its bacterial host, *lacZ* transcription is promoted in the

presence of isopropyl-beta-D-thiogalactopyranoside (IPTG), producing the enzyme galactosidase. The galactosidase enzyme specifically cleaves X-gal, producing a blue color in the bacterial colonies grown on nutrient rich agarose plates. Titering is then the process of dilution of the phage solution and immobilization of the infected bacterial hosts onto IPTG/X-gal containing agarose plates. This process ensures the reporting of single infection events as individual blue plaques on the plate, providing a quantifiable assay of isolated phage. Therefore, all concentrations of phage as determined via tittering are given in plaque forming units (PFU), and are reported with a single digit accuracy (i.e. $1x10^x$) (*22*).

1.4 *Materials Used*

The ability of phage display to extend the repertoire of materials that can be manipulated with biomolecules has been exploited to advance the synthesis of metallic, magnetic and semiconducting materials on the nanometer scale. The materials explored in the following body of work where chosen for their importance in current technologies including data storage and components in advanced circuitry (magnetic and semiconducting), and to address the issue of wiring these components into nanoscaled devices (metals). They also provide a basis set with enough complexity to assemble rudimentary components in electronic circuitry. The development of each of these systems tests the boundaries of the types of materials that can be processed utilizing biology.

1.4.1 Noble *Metals (Au, Cu, Pt)*

Noble metals serve as an integral part of today's technologies and bridge the gap between device components and electrical input (*30*). Nanoscale gold systems also exhibit plasmon properties that make them useful for detection of a variety of compounds, including DNA (*31,32*). Screening of these materials using phage display will provide a biological route for developing strategies for fabricating bio-inorganic device architectures (*33*). Noble metals where also selected because of the numerous techniques that would be available for studying these systems such as Surface Plasmon Resonance (SPR, *34*) and Surfaced Enhanced Raman Spectroscopy (SERS, *35*). Other projects aimed at understanding the interaction of peptides with the gold surface have included molecular modeling techniques (*36*) and Nuclear Magnetic Resonance (NMR) studies (*37*).

Surface Plasmon Resonance -

Since the discovery of the optical surface plasmon resonance effect by Otto in 1968 (*38*), it has found many applications in the detection of surface species. Most recently it has been widely used for the in situ monitoring of biological molecules, providing real time information on the binding kinetics and thermodynamics (*39*). The excitation of surface plasmons in a thin metal film by a polarized optical source in a total internal reflectance (TIR) geometry shows a dramatic dip in the reflected intensity at the resonance angle (*40*). This resonance angle is highly dependant on the dielectric layer directly opposite the metal glass interface, i.e. the index of refraction, and molecules binding to the metal surface on the length scale dictated by the evanescent wave created by the TIR geometry (~250nm) cause a dramatic shift in the resonance angle. This angle dependant dip in intensity, which is directly proportional to the amount of

analyte adsorbed, is detected via a photodiode or more recently, imaged on a Charged Coupled Device (*41*). SPR has proven to be an effect means of determining the time scales and thermodynamics of surface interactions (*42*), but does not provide data on specific interactions with the substrate.

NMR has produced significant results toward the understanding of ligation of gold nanoparticles in the recent literature (*43*), and is a useful avenue for understanding both peptides themselves and peptide-metal interactions.

1.4.2 *Semiconducting Materials (CdS, ZnS)*

The unique electrical properties of semiconducting materials on the nanometer scale, including GaN, Si, Cd(S,Se.Te), has spurred intense research in the synthesis of the materials with lowered dimensions including chemical (*44*) and biological routes (*45*). Most of the organo-metallic chemistry based synthetic strategies employ high temperatures and toxic chemical precursors. Using biological strategies has the potential for creating green synthetic routes that can also address current thermodynamic and chemical limitations (*46*). Evolution of substrate specific peptides through phage display technologies for the directed nucleation of materials on the nanometer scale has been previously reported and serves as the basis for the material specificity in the virus template (*13*). Screening of the ZnS and CdS (*14, 47*) systems using commercially available bacteriophage libraries (New England Biolabs) expressing either a disulphide constrained (Cys-Cys) heptapeptide or a linear dodecapeptide as a fusion to the gPIII protein located at the proximal tip of the virus has yielded nucleating peptides with the sequences: CNNPMHQNC (termed A7; ZnS), SLTPLTTSHLRS (termed J140; CdS). These peptides were incorporated into the phage scaffold described in this work to both show the

generality of the synthetic scheme and the unique electrical properties needed for designing nanoscale device elements.

It is believed that the adhesion characteristics of peptides with semiconductor surfaces stem from both the semiconductor specific electronegativity and the acidity of the amino-acid side groups within the peptide (48). These properties can be effected through changes in solution, including pH and ionic strength (49), adding an element of control over peptide-semiconductor binding events.

1.4.3 *Magnetic Materials (Co, CoPt, FePt)*

Biological organisms have evolved the ability to control the synthesis and assembly of inorganic materials through proteins under environmentally benign conditions. Several examples exist in nature of protein-mediated inorganic synthesis, and researchers have begun manipulating these organisms and proteins to synthesize inorganic materials with controlled composition and crystallinity (50). Most of these efforts have focused on preparing materials composed of sulfides (51,52,53), calcium carbonate (54,55), silicon oxide (56), iron oxides (57,58), and noble metals (59,60,61,62), but these materials are often similar to naturally-abundant, biologically prepared inorganic materials. Here we use biological interactions to control the nucleation of materials that are not isomorphous to materials found in nature.

In Stoner's 1936 treatise on the internal energy of ferromagnetics, it was predicted that a crystal domain on the order of 10^4 atoms (~10nm diameter spheres) could only support a single magnetic domain (63). Murray and co-workers at IBM's Watson Research Center have since demonstrated this unique property for 2-5nm diameter FePt and Cobalt nanoparticles (64). This 1:1 correlation between NP and magnetic moment (i.e. readable bit) makes NPs ideal candidates

for developing denser recording media. However, it has also been shown by Murray *et.al.* (*65*) that inconsistencies in NP size, shape, surface defects, and magnetocrystalline defects lead to magnetic anisotropies that render them useless for their implementation in the manufacturing of recording media. Current synthesis of FePt, CoPt, Co, FeCo and other known magnetic nanoparticles rely on the air sensitive, high temperature, and expensive polyol reduction of organometallic salts (*66*). Platinum alloy particles in particular require post synthesis annealing in order to under go a phase transition from superparamagnetic to ferromagnetic (*67*). The size and flocculation of these NPs are mediated by multi-surfactant systems and precipitation processes that lack the desired control over NP characteristics. Synthesizing NPs under peptide control provides an inexpensive route to highly ordered, defect free particles under ambient conditions (*68*).

Cobalt –

Synthesis and characterization of cobalt nanoparticles has garnered much attention in the literature over the past six years for it many size dependant properties. Although magnetic nanoparticles hold promise for medical applications, there has been significant research performed for their use in magnetic storage media (*68,69*). There has been many proposed synthetic routes for creating single domain magnetic cobalt, most notable has been the routes of Bawendi (*70*), Murray (*71*), and Alivisatos (*72*) and are based on the polyol process. The assembly of cobalt nanoparticles into well ordered structures is a promising route toward ultra-high density recording media (*73*). However, the magnetic anisotropy of cobalt is not large enough to overcome the superparamagnetic limit (*74*); the limit at which the magnetic anisotropy energy of the particles is on par with the thermal energy. At this limit, thermal fluctuations cause

random flipping of the magnetic moment, prohibiting any long term data storage capacities (75). To overcome the effect of diminishing magnetic anisotropy as particle sizes shrink, alloyed systems have been pursued due to their large magnetic moments (76).

Development of peptides that can control the nucleation of cobalt nanoparticles has been pursued as a model system for developing the methods needed to synthesize alloyed nanoparticles that have a more complex synthesis and chemical structure.

Magnetic Platinum Alloys –

The metal alloys FePt and CoPt are particularly interesting for ultra high density magnetic recording because they exhibit high magnetic anisotropy (77,78) and resist chemical oxidation. Future progress in ultra-high density magnetic data storage will depend on the development of metal thin film media with smaller particles, tighter size distributions and optimized compositions (79). This has lead several researchers to begin developing solution-based synthesis techniques for ferromagnetic nanoparticles (80,81,82) as an alternative to the sputtering techniques used for conventional media (83). These solution-based methods have proven to be excellent tools for preparing monodisperse metal nanoparticles of FePt and CoPt (84,85,86) . These particles have also been shown to crystallize into ordered face-centered cubic (FCC) and hexagonally close-packed (HCP) arrays, which can function as high density memory devices (87,88).

Although these synthetic strategies have had success in generating monodisperse, ordered arrays of CoPt and FePt nanoparticles, they are of the chemically unordered phase. In order to achieve the magnetic anisotropy needed for recording devices, these alloys must be in the chemically ordered $L1_0$ crystal phase. Because this phase is thermodynamically stable only

above 400°C and 500°C for FePt and CoPt respectively (*67*), post synthesis annealing is required. This annealing removes the protective organic layer used to stabilize the particles, and thus causes aggregation of the particles. Therefore a biological route that aims at exploiting nature's ability to nucleate metastable crystal phases at room temperature to develop a direct synthesis of $L1_o$ phase FePt and CoPt nanoparticles (figure 1.7).
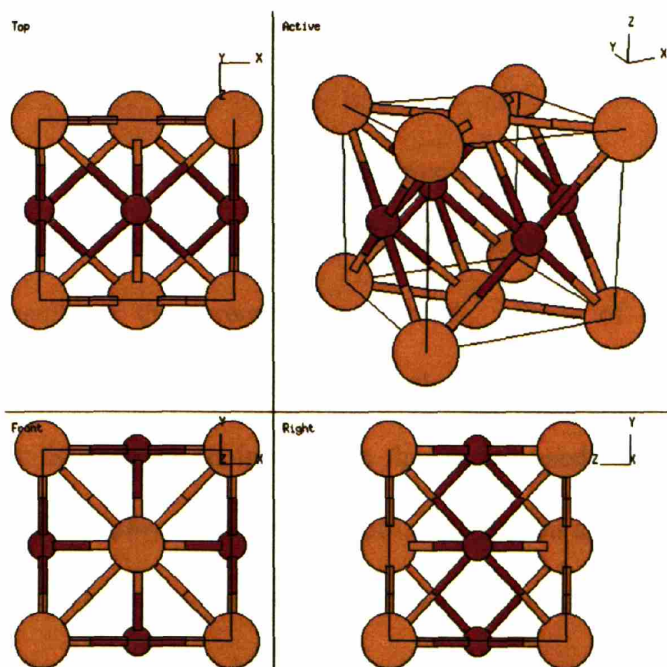
Figure 1.7 Diagram of the L10 crystal structure. Obtained from http://cst-www.nrl.navy.mil/lattice/struk.picts/l1_0.s.png

1.5 *Scope of Work*

The basis of the work presented is the ability of nature to control the synthesis of highly ordered bioinorganic structures such as bone, shells, teeth, as well as pure inorganic structures such as metallic and magnetic nanoparticles. This work seeks to utilize the knowledge gained in the field of biomineralization to expand upon the types and forms of materials that we can control using biological factors. The overall goal is to discover peptides that have similar

capabilities as naturally occurring biomineralization systems, but for materials that are not found in nature. Creation of biomineralization organisms for technologically relevant materials can then be achieved through incorporation of these peptides into biological systems. These biological scaffolds can then be developed to control the synthesis and organization of nanoscaled materials for their facile integration into next generation technologies including integrated circuitry and chemical sensors. This text describes the process of peptide selection, incorporation and function as laid out bellow.

Chapter 2 – discusses the experimental details in preparing and characterizing the substrates used during the phage display screening. It also outlines the procedures used for screening the substrates, and the results of the screening experiments. Some of the peptides discovered through the phage display process where analyzed for their binding affinities to better understand the level of specificity that can be achieved from the library used. Both tittering and surface plasmon resonance where employed on two separate systems (Co and Au respectively). Lastly, computer modeling of the peptides was performed in order to elucidate any obvious peptide-substrate interactions that could be used to better understand the mechanism behind the peptide-substrate interaction, and how it influences particle nucleation.

Chapter 3 – discusses the M13 bacteriophage scaffold in further detail, and how manipulation of its genome and perturbations to its life cycle can yield multifunctional scaffolds for materials synthesis and for programmable assembly.

Chapter 4 – discusses in detail the development of the biomineralization process used to synthesize magnetic, metallic and semiconducting nanoparticles and wires under ambient, aqueous conditions. It goes on to explore the effect of the scaffold on both the synthesis of nanoparticle and their assembly into 1 dimensional nanoparticle arrays. It also discusses the techniques developed to further process these arrays in order to produce highly crystalline free standing nanowires.

Chapter 5 – explores the development of multi functional scaffolds for synthesizing, organizing and specific placement of these structures into functional devices, testing the proof of concept that a biological system can be designed to assemble nano-architectures for future technologies.

Chapter 6 – provides an overview of the progress made in each area of the research; peptide selection; bioscaffold development; peptide driven nanoparticle synthesis; biologically organized nanoparticle arrays; and genetic coding of a nanoscale material architecture into the M13 bacteriophage.

References

1. R. de Picciotto; H.L. Stormer; L.N. Pfeiffer; K.W. Baldwin; K.W. West, Four0terminal resistance of a ballistic quantum wire. *Nature* **2001**, *411*, pp. 51-54.

2. Y. Wang; L. Zhang; C. Liang; G. Wang; X. Peng, Catalytic growth and photoluminescence properties of semiconductor single-crystal ZnS nanowires. *Chem. Phys. Lett.* **2002**, *357*, pp. 314-318.

3. Y. Huang *et. al.*, Logic gates and computation from assembled nanowire building blocks. *Science* **2001**, *294*, pp. 1313-1317.

4. A. M. Morales; C.M. Lieber, A laser ablation method for the synthesis of crystalline semiconductor nanowires. *Science* **1998**, *279*, pp. 208-211.

5. L. Manna; E. C. Scher; A. P. Alivisatos, Synthesis of soluble and processable rod-, arrow-, teardrop-, and tetrapod-shaped CdSe nanocrystals. *J. Am. Chem. Soc.* **2000**, *122*, pp. 12700-12706.

6. Y. Xia *et. al.*, One-dimensional nanostructures: synthesis, characterization, and applications. *Adv. Mat.* **2003**, *15*, pp. 353-389.

7. J. N. Cha; G. D. Stucky; D. E. Morse; T. J. Deming, Biomimetic synthesis of ordered silica structures mediated by block copolypeptides. *Nature* **2000**, *403*, pp. 289-292.

8. J. D. Hartgerink; E. Beniash; S. I, Stupp, Self-assembly and mineralization of peptide-amphiphile nanofibers. *Science* **2001**, *294*, pp. 1684-1688.

9. T. Douglas; M. Young, Host-guest encapsulation of materials by assembled virus protein cages. *Nature* **1998**, *393*, pp. 152-155.

10. E. Dujardin *et. al.*, Organization of metallic nanoparticles using tobacco mosaic virus templates. *Nano Lett.* **2003**, *3*, pp. 413-417.

11. S. Lee; C. Mao; C. E. Flynn; A. M. Belcher, Ordering of quantum dots using genetically engineered viruses. *Science* **2002**, *296*, pp.892-895.

12. M. Reches; E. Gazit, Casting metal nanowires within discrete self-assembled peptide nanotubes. *Science* **2003**, *300*, pp. 625-627.

13. S. R. Whaley; D. S. English; E. L. Hu; P. F. Barbara; A. M. Belcher, Selection of peptides with semiconductor binding specificity for directed nanocrystal assembly. *Nature* **2000**, *405*, pp. 665-668.

14. C. Mao *et. al.*, Viral assembly of oriented quantum dot nanowires. *Proc. Natl. Acad. Sci. USA* **2003**, *100*, pp. 6946-6951.

15. Naik, R.R. et. al. Peptide templates for nanoparticle synthesis derived from polymerase chain reaction-driven phage display. *Adv. Funct. Mater.*, **2004**, *14*(1), pp. 25-30.

16. *On Biomineralization*, ed. H.A. Lowenstam and S. Weiner. **1989**, Oxford: Oxford University Press.

17. Kroger, N. and M. Sumper, The Biochemistry of Silica Formation in Diatoms, in Biomineralization, E. Baeuerlein, Editor. **2000**, Wiley-VCH: Weinheim. pp. 151-170.

18. Belcher, A.M., et al., Control of crystal phase switching and orientation by soluble mollusk-shell proteins. *Nature* **1996**. *381*(6577), pp. 56-58.

19. Weiner, S.; Traub, W. Bone-Structure - from Angstroms to Microns. *Faseb Journal* **1992**, *6*(3), pp. 879-885.

20. Jackson, A.P., J.F.V. Vincent, and R.M. Turner, Comparison of nacre with Other ceramic composites. *Journal of Materials Science* **1990**. *25*(7), pp. 3173-8.

21. Bazylinski, D.A. and R.B. Frankel, Magnetic Iron Oxide and Iron Sulfide Minerals within Microorganisms, in *Biomineralization: From Biology to Biotechnology and Medical Application*, E. Baeuerlein, Editor. **2000**, Wiley-VCH: Weinheim. pp. 25-46.

22. Ph.D.-12™, Ph.D.-7™, Ph.D.-C7C™ Phage Display Peptide Library Kit Instruction Manuals, *New England Biolabs*.

23. Sidhu, S.S. Engineering M13 for phage display, *Biomolecular Engin.* **2001**, *18*, pp. 57-63.

24. Gailus, V.; Rasched, I. The adsorption protein of bacteriophage fd and its neighbor minor coat protein build a structural entity. *Euro. J. Biochem.* **1994**, *222*, pp. 927-931.

25. Sidhu, S.S.; Weiss, G.A.; Wells, J.A. High copy display of large proteins on phage for functional selections. *J. Mol. Bio.* **2000**, *296*, pp. 487-495.

26. Martin, D.A. Filamentous phage structure, infection and assembly. *Curr. Opin. Struct. Bio.* **1998**, *8*, pp. 150-158.

27. Huse, W. et. al. Generation of a large combinatorial library of immunoglobulin repertoire in phage lambda. *Science* **1989**, *246*, pp. 1275-1281.

28. Smith, G. Filamentous fusion phage: novel expression vectors that display cloned antigens on the viron surface. *Science* **1985**, *228*, 1315-1317.

29. Petrenko, V.; Smith, G.; Gong, X.; Quinn, T. A library of organic landscapes on filamentous phage. *Prot. Eng.* **1996**, *9*(9), 797-801.

30.   Yanson, A.; Bollinger, R.; van der Brom, H.; Agarait, N.; van Ruitenbeek, J. Formation and manipulation of a metallic wire of single gold atoms. *Nature* **1998**, *395*, pp.783-785.

31.   Park, S.; Taton, A.; Mirkin, C. Array-based electrical detection of DNA with nanoparticle probes. *Science* **2002**, *295*, pp. 1503-1506.

32.   Woodbury, R.G. et. al. Construction of biosensors using a gold-binding polypeptide and a minerature intergrated surface plasmon resonance sensor. *Biosernsors and Bioelectronics*, **1998**, *13*, pp. 1117-1126.

33.   Jeuken, L.J.C. et. al.   Direct electrochemical interaction between a modified gold electrode and a bacterial membrane extract. *Langmuir* **2005**, *21*(4), pp. 1481-1488.

34.   Malmborg, A.; Borrebaeck, C. BIAcore as a tool in antibody engineering. *J. Immun. Methods* **1995**, *183*, pp. 7-13.

35.   Ooka, A.; Garrell, R. Surface enhanced raman spectroscopy of DOPA-containing peptides related to adhesive protein of marine mussel, *Mytilus edulis. Biopoly.(Biospec.)* **2000**, *57*, pp. 92-102.

36.   Grater, F.; Schwarzl, S. M.; Dejaegere, A.; Fischer, S.; Smith, J. C. Protein/Ligand Binding Free Energies Calculated with Quantum Mechanics/Molecular Mechanics. *J. Phys. Chem. B.* **2005**, *109*(20), pp. 10474-10483.

37.   Kohlmann, O.; Steinmetz, W.; Mao, X.; Wuelfing, W.; Templeton, A.; Murray, R.; Johnson Jr., C. NMR diffusion, relaxation, and spectroscopic studies of water soluble, monolayer-protected gold nanoclusters. *J. Phys. Chem. B* **2001**, *105*, p. 8801-8809.

38.   Otto, A. *Z. Phys.* **1968**, *216*, 398.

39.   Malmborg, A.; Ohlin, M. Characterization of bacteriophages by the use of BIAcore and Origen analyzer. *Int. J. Bio-Chrom.* **1999**, *4*(3), pp. 163-173.

40.   Webber, W. Modulated Surface-Plasmon Resonance for *in situ* metal-film surface studies. *Phys. Rev. Lett.* **1977**, *39*(3), pp. 153-156.

41.   Stenberg, E.; Persson, B.; Roos, H.; Urbaniczky, C. Quantitative determination of surface concentration of protein with surface plasmon resonance using radiolabeled proteins. *J. Coll. Int. Sci.* **1991**, *143*(2), pp. 513-526.

42.   Malmborg, A.; Duenas, M.; Ohlin, M.; Soderlind, E.; Borrebaeck, C. Selection of binders from phage displayed antibody libraries using BIAcore biosensor. *J. Immun. Methods*, **1996**, *198*, pp. 51-57.

43.   Thomas, K.; Zajicek, J.; Kamat, P. Surface binding properties of tetraoctylammonium bromide-capped gold nanoparticles. *Langmuir* **2002**, *18*, pp. 3722-3727.

44. Cui, Y.; Wei, Q.; Park, H.; Lieber, C. Nanowire nanosensors for highly sensitive and selective detection of biological and chemical species. *Science* **2001**, *293*, pp. 1289-1292.

45. Matoussi, H.; Mauro, M.; Goldman, E.; Anderson, G,; Sundar, V.; Mikulec, F.; Bawendi, M. Self assempbly of CdSe-ZnS quantum dot bioconjugates using an engineered recombinant protein. *J. Am. Chem. Soc.* **2000**, *122*, pp. 12142-12150.

46. Sone, E.D.; Stupp, S.I. Semiconductor-encapsulated peptide-amphiphile nanofibers. *J. Am. Chem. Soc.*, **2004**, *126*, pp. 12756-12757.

47. Flynn, C.E. et. al. Synthesis and organization of nanoscale II-VI semiconductor materials using ecolved peptide specificity and viral capsid assembly. *J. Mater. Chem.*, **2003**, *13*, pp. 2414-2421.

48. Goede, K.; Busch, P.; Grundmann, M. Binding specificity of a peptide on semiconductor surfaces. *Nanoletters*, **2004**, *4*(11), pp. 2115-2120.

49. Luey, J.; McGuire, J.; Sproull, R.D. The effect of pH and NaCl concentration on adsorption of beta-lactoglobulin at hydrophilic and hydrophobic silicon surfaces. *J. Coll. Inter. Sci.*, **1991**, *143*(2), pp. 489-500.

50. Wong, K.; Douglas, T.; Gider, S.; Awschalom, D.; Mann, S. Biomimetic synthesis and characterization of magnetic proteins (magnetoferritin.) *Chem. Mater.* **1998**, *10*, pp. 279-285.

51. Wong, K. K. W. & Mann, S. Biomimetric Synthesis of Cadmium Sulfide -Ferritin Nanocomposites. *Adv. Mater.* **8**, 928-933 (1996).

52. Dameron, C. T. et al. Biosynthesis of Cadmium Sulphide Quantum Semiconductor Crystallites. *Nature* **338**, 596-597 (1989).

53. Kowshik, M., Vogel, W., Urban, J., Kulkarni, S. K. & Paknikar, K. M. Microbial Synthesis of Semiconductor PbS Nanocrystallites. *Adv. Mater.* **14**, 815-818 (2002).

54. Zaremba, C. M. et al. Critical Transformations in the Biofabrication of Abalone Shells and Flat Pearls. *Chem. Mater.* **8** (1996).

55. Falini, G., Albeck, S., Weiner, S. & Addadi, L. Control of Aragonite or Calcite Polymorphism by Mollusk Shell Macromolecules. *Science* **271**, 67-69 (1996).

56. Fowler, C. E., Shenton, W., Stubbs, G. & Mann, S. Tobacco Mosaic Virus Liquid Crystals as Templates for the Interior Design of Silica Mesophases and Nanoparticles. *Adv. Mater.* **13**, 1266-1269 (2001).

57. Douglas, T. & Stark, V. T. Nanophase Cobalt Oxyhydroxide Mineral Synthesized with the Protein Cage of Ferritin. *Inorg. Chem.* **39**, 1828-1830 (2000).

58. Shenton, W., Mann, S., Colfen, H., Bacher, A. & Fischer, M. Synthesis of Nanophase Iron Oxide in Lumazine Synthase Capsids. *Adv. Mater.* **40**, 442-445 (2001).

59. Brown, S., Sarikaya, M. & Johnson, E. A Genetic Analysis of Crystal Growth. *J. Mol. Biol.* **299**, 725-735 (2000).

60. Dujardin, E., Peet, C., Stubbs, G., Culver, J. N. & Mann, S. Organization of Metallic Nanoparticles Using Tobacco Mosaic Virus Templates. *Nanoletters* (2002).

61. Naik, R. R., Stringer, S. J., Agarwal, G., Jones, S. E. & Stone, M. O. Biomimetric Synthesis and Patterning of Silver Nanoparticles. *Nature Mater.* **1**, 169-172 (2002).

62. Mukherjee, P. et al. Fungus-Mediated Synthesis of Ag Nanoparticles and their Immobilization in the Mycelial Matrix: A Novel Biological Approach to

63. Stoner E.C. The internal energy of Ferromagnetics, *Phil. Trans. Royal Soc. London Series A, Math. And Phys. Sci.* **1936**, *235*(750), pp. 165-193.

64. Sun, S.; Murray, C.; Weller, D.; Folks, L.; Moser, A. Monodisperse FePt nanoparticles and ferromagnetic FePt nanocrystal superlattices. *Science* **2000**, *287*, pp. 1989-1992.

65. Diehl, M.R.; Yu, J.Y.; Heath, J.R.; Held, G.A.; Doyle, H.; Sun, S.; Murray, C.B. Crystalline, Shape and Surface Anisotropy in Two Crystal Morphologies of Superparamagnetic Cobalt Nanoparticles by Ferromagnetic Resonance. *J. Phys. Chem. B* **2001**, *105*, p. 7913-7919.

66. Fivet, F.; Lagier, J.P.; Figlarz, M. Preparing monodisperse metal powders in micrometer ad submicrometer sizes by the polyol process. *MRS Bulletin* **1989**, December, pp. 29-34.

67. Barmak, K. et. al. Calorimetric studies of the A1 to L1$_0$ transformation in FePt and CoPt thin films. *App. Phys. Lett.* **2002**, *80*(22), pp. 4268-4270.

68. Held, G.A.; Grinstein, G.; Doyle, H.; Sun, S.; Murray, C.B. Competing interactions in dispersions of superparamagnetic nanoparticles, *Phys. Rev. B* **2001**, *64*, 12408 (4 pages).

69. Kumbhar, A. Magnetic Properties of Cobalt and Cobalt-platinum alloy nanoparticles synthesized via microemulsion technique. *IEEE Trans. Mag.* **2001**, *37*(4), pp. 2216-2218.

70. Jamet, M. et. al. Magnetic Anisotropy of a single cobalt nanocluster. *Phys. Rev. Lett.* **2001**, *86*(20), pp. 4676-4679.

71. Dinega, D.; Bawendi, M. A solution phase chemical approach to a new crystal structure of cobalt. *Angew. Chem. Int. Ed.* **1999**, *38*(12), 1788-1791.

72.	Sun, S., Murray, C. B. & Doyle, H. Controlled Assembly of Monodisperse e-Cobalt-Based Nanocrystals. *Mat. Res. Soc. Symp. Proc.* **577**, 385-398 (1999).

73.	Puntes, V. F., Krishnan, K. M. & Alivisatos, A. P. Colloidal Nanocrystal Shape and Size Control: The Case of Cobalt. *Science* **291**, 2115-7 (2001).

74.	Sun, S.; Murray, C.B. Synthesis of monodisperse cobalt nanocrystals and their assembly into magnetic superlattices. *J. App. Phys.* **1999**, *85*(8), pp. 4325-4330.

75.	Skumryev, V.; Stoyanov, S.; Zhang, Y.; Hadjipanayis, G.; Givord, D.; Nogues, J. Beating the superparamagnetic limit with exchange bias. *Nature* **2003**, *423*, pp. 850-853.

76.	Weller, D. & Moser, A. Thermal Effect Limits in Ultrahigh-Density Magnetic Recording. *IEEE Trans. Mag.* **35**, 4423-4439 (1999).

77.	Jeong, S.; Hsu, Y.; Laughlin, D.; McHenry, M.E. Magnetic properties of nanostructured CoPt and FePt thin films. *IEEE Trans. Mag.* **2000**, *36*(5), pp. 2336-2338.

78.	Sakuma, A. First principle calculation of the magnetocrystalline anisotropy energy of FePt and CoPt ordered alloys. *J. Phys. Soc. Japan* **1994**, *63*(8), pp. 3053-3058.

79.	Chang, G.S.; Whang, C.N.; Rhee, J.Y.; Lee, Y.P. Electronic and structural properties of equiatomic Co-Pt alloy films at low temperatures. *J. App. Phys.*, **2000**, *87*(4), pp. 1775-1779.

80.	Yu, C.C.A.; Mizuno, M.; Sasaki, Y.; Kondo, H. Structural characteristics and magnetic properties of chemically synthesized CoPt nanoparticles. *App. Phys. Lett.* **2002**, *81*(20), pp. 3768-3770.

81.	Chinnasamy, C.N.; B. Jeryadevan, B.; Shinoda, K.; Tohji, K. Polyol-process-derived CoPt nanoparticles: Structural and magnetic properties. *J. App. Phys.*, **2003**, *93*(10), pp. 7583-7585.

82.	Chen, M.; Nikles, D. Synthesis of spherical FePd and CoPt nanoparticles, *J. App. Phys.* **2002**, *91*(10), pp. 8477-8479.

83.	Park, S.; Jung, P.; Kim, K. Magnetic properties and microstructural analysis of sputter-deposited and annealed CoPt alloys. *J. App. Phys.* **1995**, *77*(6), pp.2641-2647.

84.	Uba, L. et. al. Influence of the crystal structure and chemical order on the magnetic and magneto-optical properties of equiatomic CoPt alloy. *J. App. Phys.* **2002**, *91*(2), pp. 775-779.

85.	Huang, Y.; Zhang, Y.; Hadjipanayis, G.C.; Simopoulos, A.; Weller, D. Hysteresis behavior of CoPt nanoparticles. *IEEE Trans. Mag.*, **2002**, *38*(5), pp. 2604-2606.

86.   Dai, Z.R.; Sun, S.; Wang, Z.L. Phase transformation, coalescence and twinning of monodisperse FePt nanocrystals. *Nanoletters* **2001**, *1*(8), pp. 443-447.

87.   Sun, S.; Weller, D. Self assembling magnetic nanomaterials. *J. Mag. Soc. Japan* **2001**, *25*(8). pp. 1434-1440.

88.   Zeng, H. et. al. Exchange-coupled FePt nanoparticle assembly, *App. Phys. Lett.* **2002**, *80*(14), pp. 2583-2585.

2.1 *Introduction*

Previously it has been shown that polyanionic proteins isolated from abalone shells that possess a high affinity for $CaCO_3$ can be used to control the crystallization of $CaCO_3$ crystals grown *in vitro* (*1,2*). The peptides selected in these experiments which bind specifically to the screened materials may be able to exhibit similar control over the nucleation and growth of nanostructures. This approach would be comparable to the arrested precipitation techniques traditionally used to prepare inorganic nanoparticles (*3*). The key differences being: the substitution of genetically engineered phage for organic ligands, aqueous solvents, room temperature reaction conditions, and direct templating of the ordered ferromagnetic phase of FePt.

The use of the rapid peptide selection method of phage display has been used to determine materials specific amino acid sequences (*4*). Because the sequences of the peptides displayed on the surface of the bacteriophage are encoded in its DNA, the materials properties that can then be controlled by that peptide are gene-linked and therefore can be manipulated using standard biological techniques (*5*). It is therefore necesarry to develop a database of known materials binders in order to provide a toolkit from which researchers can design biological scaffolds for the synthesis and organization of multiple classes of materials.

2.2 *Phage Display Methods*

Three M13 bacteriophage libraries displaying 10^{9} random dodeca- and constrained hepta- peptides, named Ph.D. 12 and Ph.D. 7c respectively, were obtained from New England Biolabs (NEB) and used without further modification. All solutions used for the screening of

materials, known as biopanning, are given in the library protocol (6). The substrates where prepared as described in the following text and screened against both libraries to determine high surface affinity peptide sequences. Dominant sequences, discovered after multiple rounds of biopanning, were tested for their functionality as materials binders and materials synthesizers as discussed in the following chapter.

Substrates where incubated with 10uL of the original library ($10^{\wedge}12$ pfu) in Tris Buffered Saline (TBS, pH 7.5) for one hour under orbital rocking at room temperature. Tween-20 ($C_{58}H_{114}O_{26}$, M.W. 1227.54, CAS 9005-64-5), a non-ionic surfactant, was added to the solution buffer in increasing concentrations (from 0.1-0.5%) during subsequent rounds of screening to interrupt non specific interactions; effectively increasing the stringency of the phage selections. After the incubation period, the substrates where removed and washed ten times with TBS containing 0.1-0.5% Tween 20 (0.1-0.5% TBST) to remove non specific binding phage. After thorough washing, the bound phage were removed from the substrate using 1mL of a general elution buffer, 0.2M Glycine-HCl (pH 2.2), known to nonspecifically disrupt phage binding interactions, for 5min. (6). Rapid neutralization of the phage containing elution buffer with 150uL of 1M Tris-HCl (pH 9.1) prevented any deleterious effects of the acidic environment on the phage. Ten fold dilutions of the neutralized eluate were prepared in TBS ($10^{\wedge}1$-$10^{\wedge}4$) using aerosol-resistant tips to prevent cross contamination. 10uL of each dilution was then added to 200uL of an e. coli culture having an optical density at 600nm (O.D. $_{600}$) of 0.5, known as the mid-log phase. The culture was prepared by inoculating 5-10mL of Langmuir Broth (LB), having the appropriate antibiotic (in this case, tetracycline), with a single colony of the ER2738 strain of the bacteria *Escherichia coli*. The infected cells where then tittered on agarose plates containing IPTG/x-gal. The original elution was then amplified using a one-hundred fold

dilution of an overnight ER2738 culture in LB, and was titerd in a similar fashion (with dilutions of 10^8-10^{11}) to prepare a solution of 10^{12} PFU's. This enriched library was then incubated with a fresh substrate, with the biopanning process being repeated through five rounds of selection. In order to increase the stringency of the selection process in subsequent rounds, the concentration of tween used during the incubation and wash steps was gradually increased. Tween-20 is commonly used to disrupt non-specific phage interactions and phage-phage interactions. After the third and subsequent rounds of selection, individual blue plaques from the eluate titer where isolated and prepared for DNA sequencing of the phage genome in order to determine the amino acid sequence of the displayed peptide. Ten Blue plaques were removed from the agarose plate using a sterile lance (either a toothpick of pipette tip) and amplified in a one-hundred fold dilution of an overnight culture of ER2738 in fresh LB for 4.5 hours. After amplification, the bacterial host was separated from the phage through centrifugation. The isolated, amplified, phage where then precipitated using the process of pegylation (7). Pegylation is the attachment of Poly(ethylene glycol) (M.W. 8000, CAS 25322-68-3) to a biological factor, in this case it serves to add additional drag and weight needed for the phage to be pulled down from solution using centrifugation. Specifically addition of an aqueous solution of 20% w/v Poly(ethylene glycol) and 2.5M NaCl at a ratio of 6:1 of the original volume, and incubated at 4°C overnight to allow for full precipitation of the phage. The phage precipitate was then isolated from solution by centrifugation. The resulting pellet was then resuspended in a sodium iodide buffer (10mM Tris-HCL, mM EDTA, 4M NaI) to extract the DNA from the phage. Ethanol precipitation of the DNA, followed by centrifugation was used to isolate the DNA which was then resuspended in sterile, type one water (having a resistivity of at least 18MOhms.) The DNA was then sequenced by the Institute for cellular and micro biology core facilities at University of

Texas, Austin, using a -96gIII primer (6). DNA sequences of the displayed peptide where then translated using the standard genetic code to determine the amino acid structure. The translated sequences where analyzed to determine dominant motifs in the sequenced peptides.

2.3 *Substrates*

The substrates screened were chosen as to increase the number and types of materials for which there were known, functional peptides. Previous studies had already determined binding sequences for the semiconducting materials GaAs; GaN; ZnS; CdS; the insulating materials CaCo3; and the magnetic material Fe3O4 (*4,5,8,9*). Any research presented in which a biological-materials interaction is used for any of the aforementioned materials relies on the peptides previously discovered. The materials screened in this work had the disadvantage that they were not isomorphous with any known naturally occurring biomineralization product. In order to test the range of materials for which the phage display method was applicable, the ferromagnetic metal Co, and the ferromagnetic metal alloys CoPt and FePt where chosen. As the research progressed, it became our goal to use the phage both as a screening vehicle and as a biological scaffold for programmable self assembly of biologically synthesized materials. To this end it was necessary to screen contact materials used in planar technologies as a means of wiring in the phage. The screening of the Noble metals gold, copper, and platinum provided a materials selection for the future design of multi-component devices. The selection of a gold binding peptide also allowed for the use of spectroscopic techniques to be used to study the binding strengths of the peptide-substrate interactions, as a means of understanding the limits of selectivity obtainable using phage display.

2.3.1 *Magnetic Materials*

2.3.1.1 *Cobalt (Co)*

Cobalt substrates where prepared by drop coating silicon wafers with Co nanoparticles under inert atmosphere, followed by thermal annealing (300°C, under 5%H_2(g)) to achieve thin films of the ferromagnetic HCP phase. Synthesis of Cobalt nanoparticles was achieved through a modified version of the polyol based strategy developed by Alivisatos (*10*). In short, this method involves the rapid thermal decomposition of an organometallic precursor containing a zero-valent metal center in the presence of a cooperative surfactant system. Specifically, using standard airless techniques, a solution of Octacarbonyldicobalt (0.6g, $C_8O_8Co_2$, M.W. 341.9, CAS 10210-68-1) and dichlorobenzene (3mL, $C_6H_4Cl_2$, M.W. 245.5, CAS 106-46-7), and rapidly injected into a surfactant mixture of oleic acid (0.2 mL, $CH_3(CH_2)_7CHCH(CH_2)_7COOH$, M.W. 282.58, CAS 112-80-1) and Trioctylphosphine Oxide (TOPO, 0.4g, $[CH3(CH2)7]3PO$, M.W. 386.65, CAS 78-50-2), dissolved in dichlorbenzene (12mL), at 182°C followed by refluxing for 30 minutes. The solution was allowed to cool to room temperature by removal of the heating mantle. Post synthesis processing involved the ethanol induced precipitation and centrifugation of the reaction product, followed by resuspension in hexane. This process was repeated thrice in order to further focus the size distribution of the cobalt nanoparticles. Verification of the synthetic process was achieved by transmission electron microscopy (TEM) and X-ray diffraction (XRD, figure 2.1). TEM samples were prepared by direct deposition of the cobalt particle solution onto carbon coated copper TEM grids (ted pella) and analyzed using a JEOL 200 cx microscope. XRD samples were prepared by drop coating aliquots of the particle solution onto 2cm^2 pieces of silicon 110, followed by drying and then repeating the process

multiple times in order to achieve the particle density necessary for achieving an accepted signal count. Analysis was performed on a Phillips XRD using the Copper K-alpha line.
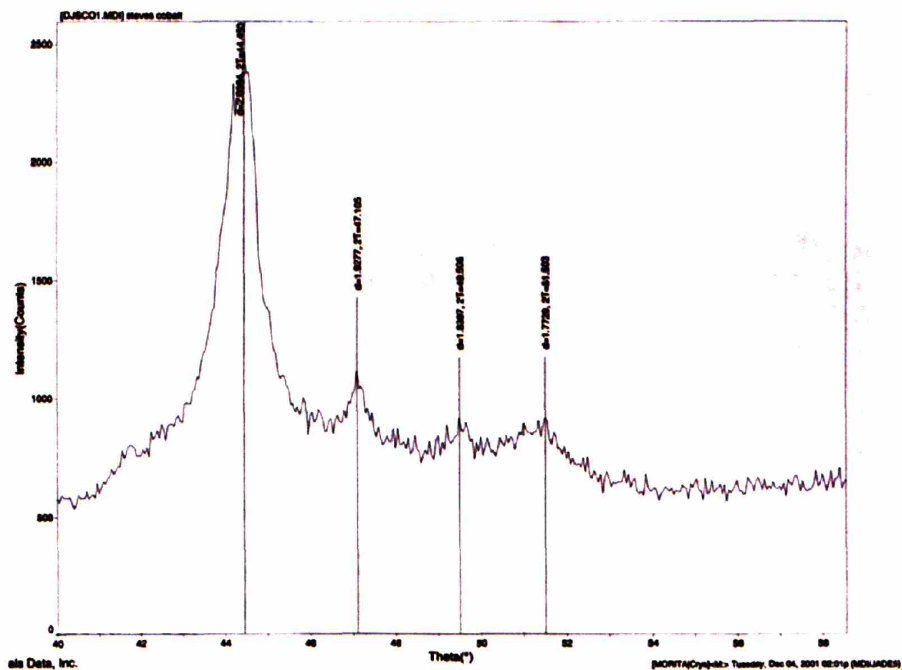
Figure 2.1 XRD of chemically synthesized Cobalt nanoparticles.

Substrates used in the screening of the phage display library were used immediately after removal from the furnace to prevent the onset of oxidation. All solutions used during the selection process were deairated under house vacuum to prevent oxidation. biopanning was performed with both the Ph.D. 12 library and yielded the sequences given in table 2.1, amino acids are color coded according to the reactivity of their side group: Hydrophobic (red); Hydrophilic (green); Negative (black); Positive (blue). All sequences are reported in order from N-terminus to C-terminus.

Table 2.1 Cobalt binding Sequences from the Ph.D. 12 library.

	Sequence											
Round 3	A	Y	Q	G	P	A	T	Q	T	W	Q	L
	G	L	S	F	Q	R	E	Q	L	Q	A	S
	N	S	Q	T	T	A	P	I	P	L	S	L
	G	N	T	S	S	L	S	Y	S	R	T	G
	S	L	Y	S	P	A	A	L	G	I	P	V
	I	S	T	P	L	G	A	S	A	P	F	K
	W	E	T	N	N	A	P	G	L	R	P	A
	H	G	S	N	W	T	H	N	N	L	G	L
	W	E	T	N	N	A	P	G	W	R	P	A
	S	P	I	A	S	Y	P	P	P	A	S	P
Round 4	G	L	S	Q	H	A	P	G	V	S	S	Y
	A	L	S	P	H	S	A	P	L	T	L	Y
Round 5	S	H	S	P	F	E	S	Q	R	I	G	L
	D	A	S	Q	M	S	S	P	S	G	M	T
	V	Y	G	K	H	N	K	P	P	P	H	S
	I	N	T	P	H	S	S	K	P	T	S	I
	I	V	Q	T	P	P	A	L	S	P	H	T
	T	P	P	A	P	G	M	M	I	S	Y	R
	I	N	T	P	H	S	S	K	P	T	S	I
	A	P	K	F	G	P	P	L	L	Q	T	P
	A	L	S	P	H	S	A	P	L	T	L	Y
	A	L	S	P	H	S	A	P	L	T	L	Y

2.3.1.2 Cobalt Platinum (CoPt)

CoPt substrates of the desired $L1_0$ phase were prepared by drop coating silicon wafers with FCC CoPt nanoparticles followed by thermal annealing (550°C). CoPt nanoparticle films were synthesized based on the polyol derived methods of Murray et. al. (*11*) and involved the simultaneous thermal decomposition of octacarbonyl dicobalt and the diol reduction of platinum acetylacetonate in the presence of the cooperative stabilizers, oleic acid and oleyl amine. Specifically, using standard airless techniques, Platinum acetalacetonate (0.5mM,) and 1,2

hexadecanediol (1.5mM) were dissolved in dioctylether(20mL) and heated to 100°C to remove any dissolved water. A solution of oleic acid (0.5mM), oleyl amine (0.5mM) and octacarbonyl dicobalt (0.5mM) was added to the reaction vessel and the entire contents were heated to 297°C, under constant stirring, and allowed to reflux for 30 minutes before removal of the heating mantle. After the solution had cooled to room temperature the reaction vessel could be opened to the atmosphere for collection of the product. Ethanol precipitation followed by centrifugation and resuspension in hexane removed any unwanted reaction byproducts and yielded monodisperse CoPt nanoparticles (~5nm) as confirmed by TEM and XRD analysis. Annealing of silicon wafer coated with the CoPt nanoparticle solution was carried out at 550°C with a ramp rate of 5 deg/min and a dwell time of 60min. The furnace was kept under a positive pressure of forming gas (5% H2) to prevent the onset of oxidation of the films. Annealing at 550°C promotes the phase transition between the FCC disordered phase of the as synthesized particles to the ferromagnetic $L1_0$ phase desired for magnetic applications.

The alloying of cobalt with platinum not only increases its magnetic anisotropy, it also adds the inert chemical properties of platinum, thus elevating the rapid oxidation commonly found in pure cobalt systems (*12*). This chemical stability to oxidation allowed for easier handling in the buffer solutions used during the panning experiments. Selection was performed as previously described in the phage display methods section and the results of the Ph.D. 12 and Ph.D. 7c screenings are given in tables 2.2 and 2.3 respectively.

Table 2.2 Cobalt Platinum Binding Sequences from the Ph.D. 12 library

	Sequence											
Round 3	V	D	S	A	N	T	T	V	S	S	S	I
	D	T	P	P	T	K	Q	M	S	F	I	F
	H	F	K	P	L	L	Y	F	G	G	S	A
	H	L	A	L	H	A	P	A	W	P	P	G
	S	P	S	M	W	P	Y	A	P	V	R	I
	V	I	T	Q	H	P	P	P	L	A	F	X
Round 4	T	M	G	F	T	A	P	R	F	P	H	Y
	H	V	L	Q	A	Q	H	P	F	V	A	W
	S	L	Y	Q	Q	A	P	H	P	P	T	M
	K	T	H	E	I	H	S	P	L	L	H	K
	H	K	Y	V	H	Q	E	S	V	W	N	L
Round 5	A	G	N	A	H	K	S	G	L	N	F	H
	T	P	P	A	P	G	M	M	I	S	Y	R
	L	N	L	P	N	T	L	P	I	G	T	R

Table 2.3 Cobalt Platinum Binding Sequences from the Ph.D. 7c library

	Sequence								
Round 3	C	S	P	T	S	A	A	L	C
	C	N	A	G	D	H	A	N	C
	C	N	A	G	D	H	A	N	C
	C	P	P	S	F	H	H	A	C
	C	E	R	G	L	H	G	N	C
	C	D	G	L	I	K	M	N	C
Round 4	C	M	P	H	M	A	R	N	C
	C	H	S	L	R	P	N	L	C
	C	L	H	G	G	Y	R	Y	C
	C	S	G	Q	N	H	W	H	C
Round 5	C	S	P	L	M	P	A	H	C
	C	K	P	F	L	H	A	Q	C
	C	X	H	N	L	K	P	T	C

2.3.1.3 *Iron Platinum (FePt)*

FePt substrates of the desired $L1_0$ phase were prepared by drop coating silicon wafers with FCC FePt nanoparticles followed by thermal annealing (550°C). FePt nanoparticle films were synthesized based on the polyol derived methods of Murray et. al. (*11*) and involved the simultaneous thermal decomposition of a Iron pentacarbonyl and the diol reduction of Platinum acetylacetonate in the presence of cooperative particle stabilizers, oleic acid and oleyl amine. Specifically, using standard airless techniques, Platinum acetalacetonate (0.5mM, sigma) and 1,2 Hexadecanediol (1.5mM) were dissolved in Dioctylether(20mL) and heated to 100°C to remove any dissolved water. A solution of Oleic acid (0.5mM), Oleyl amine (0.5mM) and Iron pentacarbonyl (1mM) was added to the reaction vessel and the entire contents were heated to 297°C, under constant stirring, and allowed to reflux for 30 minutes before removal of the heating mantle. After the solution had cooled to room temperature the reaction vessel could be opened to the atmosphere for collection of the product. Ethanol precipitation followed by centrifugation and resuspension in hexane removed any unwanted reaction byproducts and yielded monodisperse FePt nanoparticles (~5nm) as confirmed by TEM and XRD analysis (figure2.2). Annealing of silicon wafer coated with the FePt nanoparticle solution was carried out at 550°C with a ramp rate of 5 deg/min and a dwell time of 60min. The furnace was kept under a positive pressure of forming gas (5% H2) to prevent the onset of oxidation of the films. Annealing at 550°C promotes the phase transition between the FCC disordered phase of the as synthesized particles to the ferromagnetic $L1_0$ phase desired for magnetic applications.
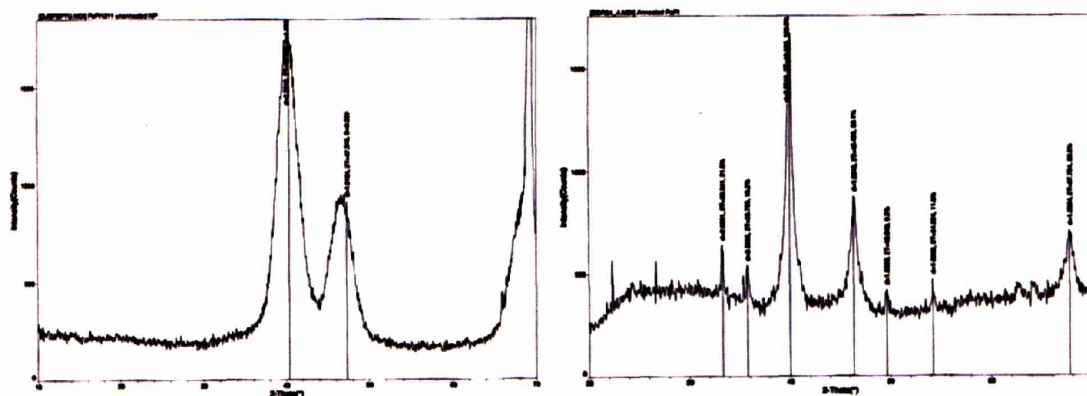
Figure 2.2 XRD analysis of Pre (left) and post (right) annealed chemically synthesized FePt nanoparticles.

Selection was performed on previously described in the phage display methods section and the results of the Ph.D. 12 and Ph.D. 7c screenings are given in tables 2.4 and 2.5, respectively.

Table 2.4 Iron Platinum binding sequences from the Ph.D. 12 library

	Sequence											
Round 4	N	G	Q	I	P	Q	L	S	H	F	P	S
	S	A	P	P	T	P	Y	Q	L	P	A	L
	A	H	R	H	P	I	S	F	L	S	T	L
	G	S	P	G	H	H	H	H	H	P	D	R
	H	N	K	H	L	P	S	T	Q	P	L	A
	G	P	H	H	K	N	E	P	H	R	H	G
	H	K	P	Q	K	P	P	S	P	H	L	L
	N	R	N	V	E	T	P	L	L	R	N	L
	P	L	R	P	E	P	V	Q	T	L	H	N
	H	N	K	H	L	P	S	T	Q	P	L	A
Round 5	L	P	N	G	Y	H	Q	R	G	L	L	X
	H	N	K	H	L	P	S	T	Q	P	L	A
	S	V	S	V	G	M	K	P	S	P	R	P
	S	V	S	V	G	M	K	P	S	P	R	P
	N	G	Q	I	P	Q	L	S	H	F	P	S
	H	T	K	P	I	N	P	K	L	L	R	Y
	X	S	R	X	X	F	L	A	P	L	G	W
	L	F	L	L	X	X	X	P	S	P	R	P
	H	G	K	I	K	E	P	R	H	V	E	A
	S	L	W	P	P	K	A	Y	F	S	F	S

Table 2.5 Iron Platinum binding sequences from the Ph.D. 7c library

	Sequence								
Round 3	C	S	F	P	H	G	T	L	C
	C	M	N	K	S	P	L	R	C
	C	T	A	A	Q	N	K	Y	C
	C	M	N	K	S	P	L	R	C
	C	G	D	M	V	D	S	T	C
	C	I	W	N	N	P	V	R	C
Round 4	C	D	G	A	P	R	T	S	C
	C	Q	A	P	S	S	L	Q	C
	C	T	T	P	L	L	P	R	C
	C	R	T	E	P	G	L	M	C
Round 5	C	P	S	L	P	N	K	H	C
	C	S	Q	L	G	P	K	S	C
	C	H	T	T	A	S	K	M	C
	C	Q	S	T	Q	A	N	S	C

2.3.2 Noble Metals

2.3.2.1 Gold (Au)

A 111 oriented single crystal gold ingot of 1cm in diameter and 0.5 cm in thickness was purchased from gmbh for screening with the phage display library. X-ray analysis confirmed the orientation of the crystal surface (figure 2.3). During the selection, the crystal was cleaned between subsequent rounds with ethanol, dried and stored under nitrogen while not in use. Between different selections the crystal was polished using a Buehler minimet polishing system (Buehler Ltd., 41 Waukegan Road, Lake Bluff, Illinois 60044, USA) with a final polish solution of 0.5um diamond paste. To obtain a surface roughness less than 0.5um, a dilute solution of potassium iodide was used as a chemical polish.
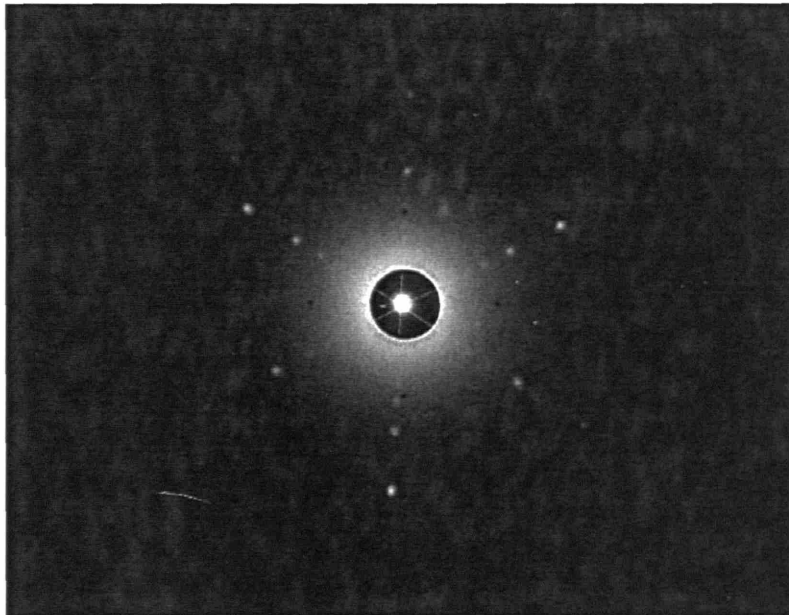
Figure 2.4 XRD diffraction pattern of the gold ingot showing the 111 reflection of the HCP crystal structure.

The selection proceeded as previously described in the phage display methods section with the only notable change being the selective elution from the crystal surface only. This was done by using the surface tension of the crystal to hold an aliquot of the elution buffer. This was done to minimize binding events due to surface defects of the rough sides of the crystal and to enrich the specific interaction with the (111) surface. The results of the screening with the Ph.D. 12 and Ph.D. 7c libraries are given in tables 2.6 and 2.7, respectively.

Table 2.6 Gold binding sequences from the Ph.D.12 library

	Sequence											
Round 3	A	L	P	A	A	Y	A	H	T	P	Q	E
	D	G	D	H	L	R	Q	A	P	N	H	W
	N	G	L	S	H	X	V	S	R	L	P	V
	S	A	N	P	E	S	Q	L	P	H	R	P
	G	L	E	H	N	Q	P	S	P	G	L	N
	D	V	S	L	S	K	R	L	E	R	P	S
	L	T	L	D	P	I	A	K	R	P	Y	S
	V	N	N	T	T	V	S	P	E	H	H	T
	E	S	S	S	K	Y	S	A	L	R	G	H
	V	N	K	T	T	V	S	P	E	H	H	T
	L	T	N	S	T	S	H	L	T	T	Y	R
	H	S	L	F	H	Q	P	S	K	Q	H	R
Round 4	L	Q	A	H	L	P	P	S	R	L	W	X
	F	D	H	T	S	T	T	L	H	K	E	V
	T	V	S	A	P	A	I	T	R	S	T	P
	L	K	A	H	L	P	P	S	R	L	P	S
	L	K	A	H	W	P	P	S	R	L	P	S
	L	K	A	H	W	L	L	S	R	L	P	S
Round 5	F	D	H	T	S	T	T	L	H	K	E	V
	L	K	A	H	L	P	P	S	R	L	P	S
	W	K	A	H	L	P	P	S	R	L	P	S
	L	K	A	H	L	P	P	R	R	L	P	S

Table 2.7 Gold Binding sequences from the Ph.D. 7c library

	Sequence								
Round 3	C	S	F	Q	S	P	R	S	C
	C	H	I	K	N	Q	N	L	C
	C	E	F	S	T	S	G	L	C
	C	E	P	K	Y	S	Q	L	C
	C	F	P	H	E	L	R	L	C
	C	P	N	T	L	Q	P	T	C
	C	P	Y	T	P	H	S	H	C
	C	G	H	Q	G	W	P	I	C
Round 4	C	F	I	S	Y	S	K	R	C
	C	S	W	T	A	F	M	S	C
	C	T	P	S	W	S	S	M	C
	C	P	N	A	S	S	T	S	C
	C	L	L	L	S	P	Q	K	C
	C	V	H	S	I	N	K	R	C
	C	S	S	E	N	N	G	Y	C
	C	L	V	N	S	A	R	V	C
	C	S	V	K	Q	V	P	V	C
	C	D	H	R	A	H	P	L	C
Round 5	C	L	P	P	G	V	A	R	C
	C	L	P	P	G	V	A	R	C
	C	V	T	N	K	T	S	Y	C
	C	P	T	G	H	K	L	P	C
	C	R	Q	P	P	Y	P	H	C
	C	S	H	K	N	T	K	Y	C
	C	K	P	S	Q	L	Y	S	C
	C	E	L	N	R	L	H	A	C

2.3.2.2 Platinum (Pt)

Platinum foil was purchased from Alfa aesar and had a chemical purity of 99.99%. The foil was annealed under argon at 400°C with a ramp rate of 5deg/min and a dwell time of 120 minutes to decrease surface roughness which also promoted the 220 crystal face as determined by XRD (figure 2.4).
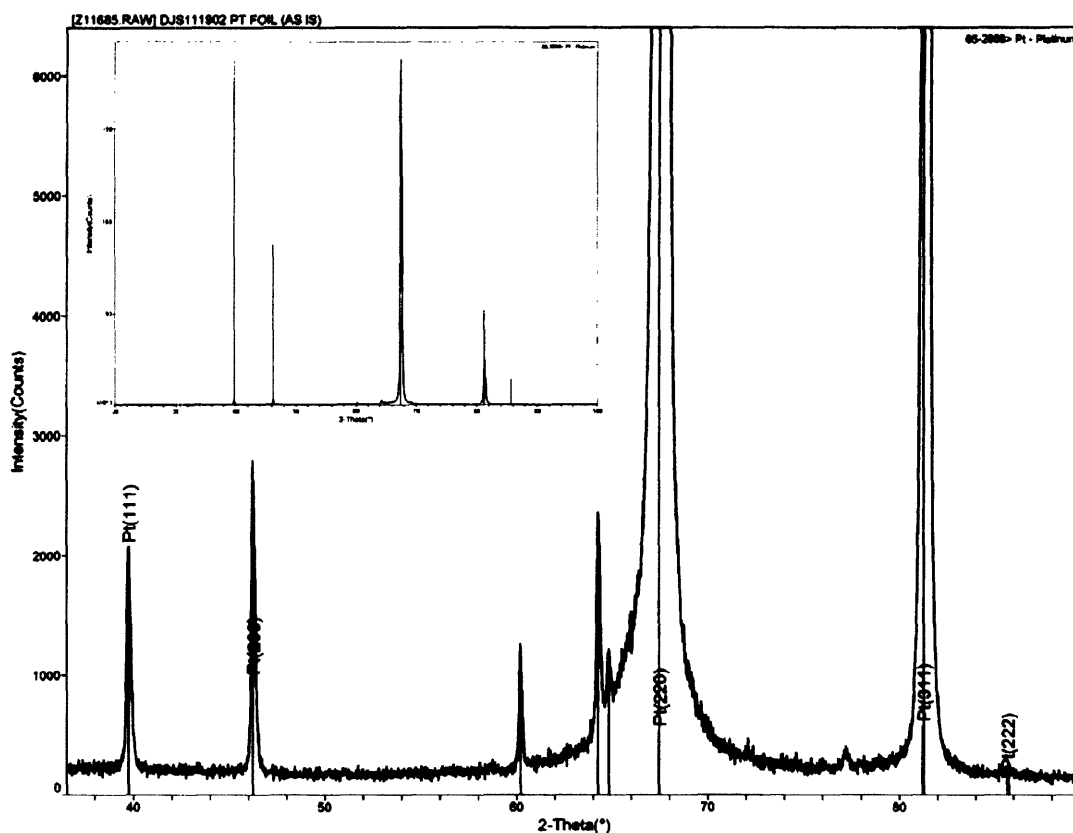
Figure 2.4 XRD pattern of the Pt foil used for library screening. Full peak intensities are shown in the insert.

Cleaning of the foil between subsequent rounds of the selection was performed by flaming the sample with a Bunsen burner followed by rinsing with ethanol and repeated three times. Screening was carried out with the Ph.D. 12 library previously described in the phage display methods section and the results are given in table 2.8.

Table 2.8 Platinum binding sequences from the Ph.D. 12 library

	Sequence											
Round 3	T	A	Y	H	R	N	T	L	P	H	L	A
	T	A	Y	H	R	N	T	L	P	H	L	A
	P	L	H	L	P	D	T	Q	A	R	P	S
	S	L	D	G	K	P	L	P	S	P	G	T
	S	L	P	A	S	T	S	T	K	N	H	V
	G	P	G	V	P	L	S	L	M	N	K	T
Round 4	P	Q	P	A	P	T	R	L	H	H	P	N
	V	P	L	T	M	A	L	R	N	P	T	A
	A	F	L	A	A	P	T	S	M	R	P	V
	A	V	P	Q	R	M	P	K	P	P	L	V
	G	P	G	V	P	L	S	L	M	N	K	T
Round 5	Y	L	E	L	S	S	K	G	P	G	P	S
	P	Q	P	A	P	T	R	L	H	H	P	N
	S	P	R	Y	T	S	T	H	L	P	S	F
	G	P	G	V	P	L	S	L	M	N	K	T

2.3.2.3 Copper (Cu)

A (111) oriented single crystal copper ingot of 1cm in diameter and 0.5 cm in thickness was received as a gift from the Professor Campion, the University of Texas at Austin, Department of Chemistry and Biochemistry, for screening with the phage display library. During the selection, the crystal was cleaned between subsequent rounds with ethanol, and dried and stored under nitrogen while not in use. Between different selections the crystal was polished using a Buehler minimet polishing system with a final polish solution of 0.5um diamond paste. The selection proceeded as previously described in the phage display methods section with the only notable change being the selective elution from the crystal surface only. This was done by using the surface tension of the crystal to hold an aliquot of the elution buffer to minimize binding events due to surface defects of the rough sides of the crystal and to enrich the specific interaction with the (111) surface. Screening of the copper surface yielded no phage. The dissolution of copper ions into solution killed all phage activity and function. The effect of

copper ions from the surface was verified by UV/Vis absorption spectroscopy (figure 2.5). Phage in TBS, that had been exposed to the copper crystal were compared to known concentrations of $CuCl_2$. According to the results, copper is electrolessly dissolved into solution on the order of 100mM.
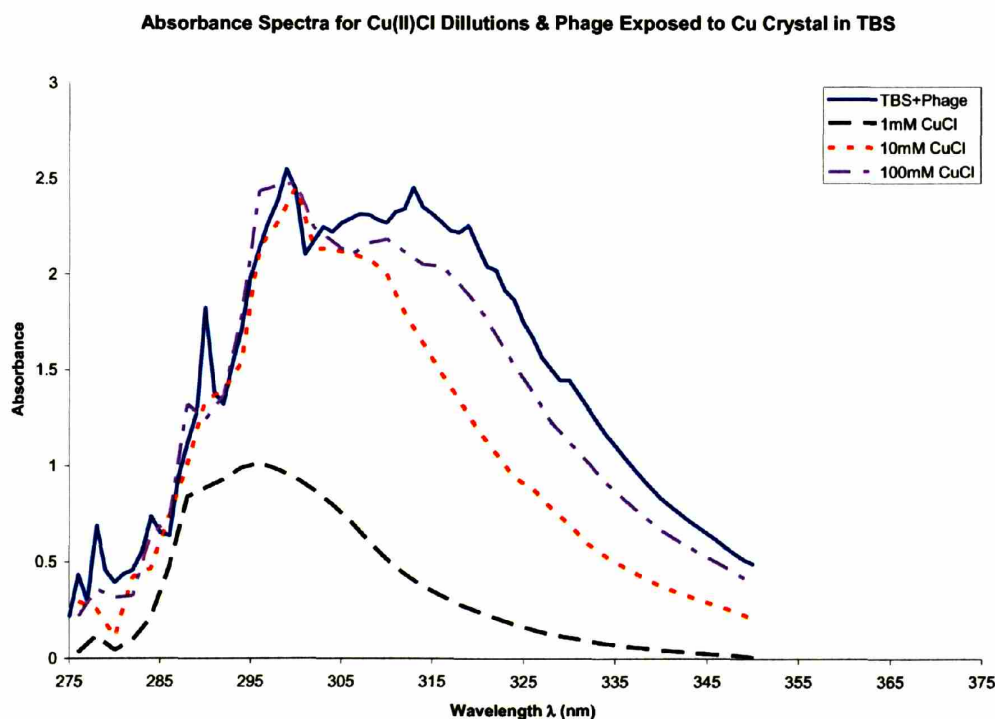
Absorbance Spectra for Cu(II)Cl Dillutions & Phage Exposed to Cu Crystal in TBS

Figure 2.5 UV/Vis adsorption spectrum of the eluate from the peptide library screening of the Cu (111) surface (solid) and standard dilutions of CoCl2.

2.4 *Discussion*

Magnetic Materials –

The magnetic materials screened were the $L1_0$ phases of CoPt and FePt, and the HCP phase of Cobalt. After five rounds of screening, dominant sequences emerged from the phage display process. The CoPt screening process yielded a peptide with the sequence KTHEIHSPLLHK, for FePt the sequence was HNKHLPSTQPLA, and for cobalt the sequence

was ALSPHSAPLTLY. The sequences for CoPt and FePt contain numerous amines, which are known to be excellent ligands for platinum, and lysine in particular is believed to be essential in the mechanism of the binding of HMG domain proteins to the Pt/DNA complex formed in cisplatin-based cancer therapies (13). Additionally, there are several examples in the literature of using Pt salts to bind histidine residues for studying protein activity (14,15) and for staining proteins with heavy metals to facilitate x-ray crystallography. Performing BLAST searches on these proteins yielded interesting results. Both of these proteins possess similarities with numerous naturally occurring proteins. For example, the metal binding protein Fe (III)-coprogen receptor of *salmonella typhimurium* contains the peptide sequence KHLPST (16) This sequence is identical to the central section of the FePt-specific dodecapeptide isolated in these experiments, and the CoPt-specific dodecapeptide contains the sequence SPLLHK, which is an identical sequence expressed in the opposite order with the addition of an extra leucine. The KHLPST sequence can also be found in pilin, a fiber-forming protein found in *e. coli* and numerous other microorganisms (17) Additionally, Co transport proteins contain numerous, alternating histidine residues, which are known to bind Co^{+2} (18), and which is a similar primary structure to the CoPt-specific dodecapeptide isolated in these experiments. The cobalt sequence on the other hand has no lysine residues, but does contain the H, L, P, S, T residues believed to be responsible for the Co^{+2} binding in these peptides. Its side groups are dominated by hydroxyl groups that may interact with an oxide layer on the substrate surface.

Noble Metals –

The Noble metals screened were the (111) face of both gold and copper, and the (220) face of platinum. The reactivity of the copper surface, combined with the interference of the free

copper ions with the phage biology, prohibited biopanning. The gold binding sequence LKAHLPPSRLPS has numerous positive amine side groups that are forced into the same plane by the double proline residue located in the center of the peptide. These groups are known binders for gold, especially on the histadine residue (*19*). Proline residues are also known binders for Ag^+, and may also play a role in the binding mechanism (*20*).

2.5 Characterization of functional peptides

2.5.1 Binding Affinities

In order to asses the level of selection capable using the phage display system on both the magnetic and noble systems discussed above adsorption isotherms were obtained for cobalt and gold using tittering and Surface Plasmon Resonance analysis, respectively. Both methods yielded plots of equilibrium surface concentration versus solution concentration. This data was fit using a mathematical model of the Langmuir isotherm $y = \left(C_{eq} \times a\right)/\left(C_{eq} + b\right)$ were the binding constant K_D is taken to be the ratio of b/a (*21*). Minimization of adsorbate-adsorbate interactions by the use of Tween-20 was used to more accurately fit the system into the Langmuir model.

Titering Isotherms –

Because tittering provides solution concentrations of phage, the relative number of surface binders can be determined. Phage expressing the cobalt functional sequence as a fusion to the gPIII were amplified, tittered, and diluted to known concentrations. Interaction of these stock solutions with cobalt substrates for one hour was followed by tittering of the solution. The difference between the number of phage put into the system and that which was collected was used to determine the equilibrium surface concentration. Fitting of the data with a mathematical

model of the langmuir isotherm yielded a binding constant on the order of 17pM (figure 2.6). Titering does not provide a highly accurate count of phage, and it is therefore difficult to achieve a quantitative binding constant. Because of this Surface Plasmon resonance and spectroscopic determination of phage combination was used to further understand the degree of phage-substrate interactions.
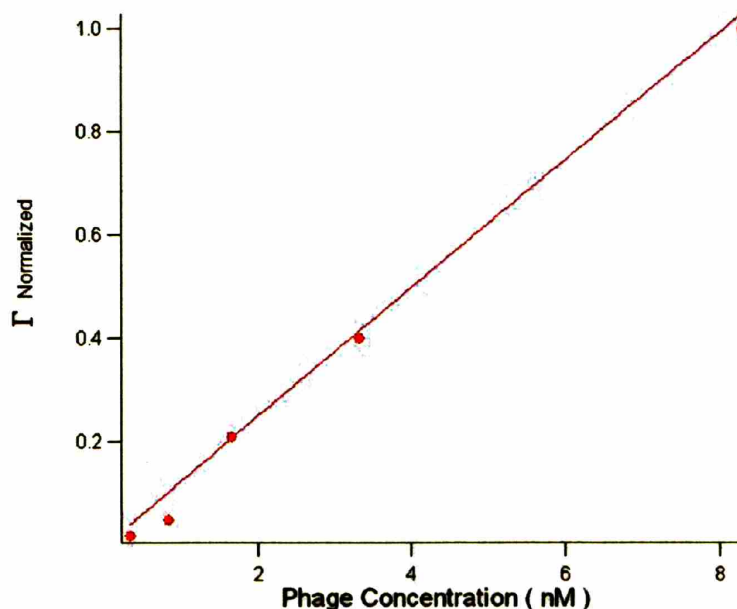

Figure 2.6 Adsorption isotherm of the Cobalt binding peptide as determined by the tittering method.

SPR Isotherms –

Surface plasmon resonance responses were collected on a thermally evaporated gold substrate (biacore SPA100) that had been cleaned overnight in gly-HCl (pH 2.2) with sonication(15min) and then seasoned overnight in TBST Running Buffer with sonication (30min). Sensograms where collected at a flow rate of 4uL/min of sonicated, filtered and degassed TBST buffer (pH 7.5), and samples where run under the kinject method with an injection volume of 40uL per sample. A virus expressing the gold binding dodecapeptide as fusion to the gPIII was amplified and purified for analysis (figure 2.7). Also, a randomly selected

phage expressing a gPIII dodecapeptide from the same library as the gold binding phage was analyzed and used to isolate the affinity of the gPIII fusion peptide from any binding effects of the gPVIII capsid; solutions were prepared in the same manner. Each of the five concentrations of the gold binding clone (0.7, 1.3, 1.9, 2.6, 7.8 nM) were repeated three times and yielded extremely reproducible results, on the basis that the sample be thoroughly mixed before injection (the standard deviation of the first two samples being higher than for the remainders for this reason.) Because of the reproducibility of the biacore 2000, the control experiments where only run once per dilution of the randomly selected peptide displaying phage. Concentration of the stock solutions were determined both by solid weight and by UV spectrophotometry at 269nm (*22*). Data was collected on a PC and analyzed using the biacore software and igor pro graphing package.
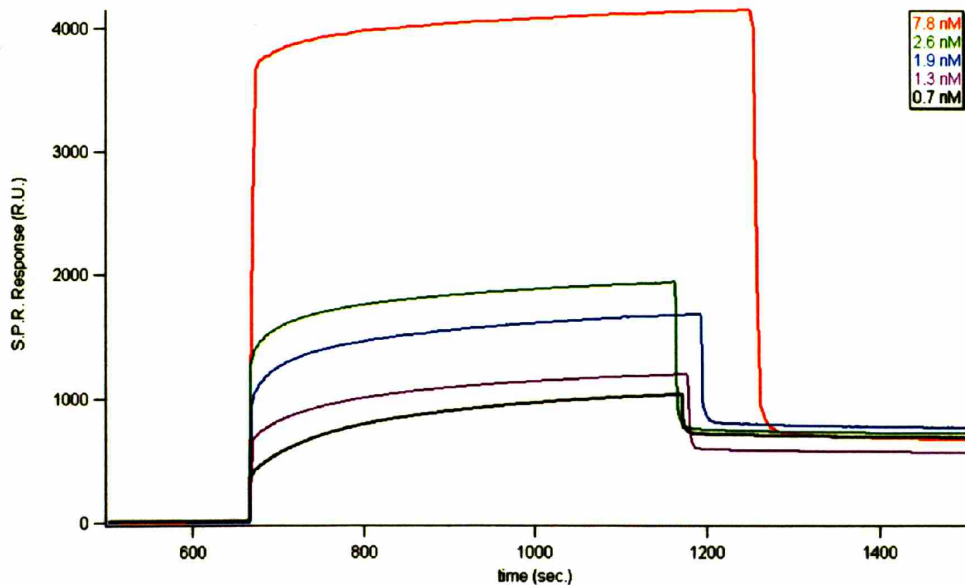

Figure 2.7 SPR sensograms of the bacteriophage displaying the gold binding dodecapeptide.

The recorded sensograms where averaged and the equilibrium surface concentrations were recorded as the maximum signal during exposure of the analyte to the surface. A fit of the data using a mathematical representation of the langmuir isotherm showed a twenty fold increase in binding affinity of the gold specific peptide over that of the randomly selected phage displaying the peptide sequence SPIASYPPPASP (figure 2.8). The values calculated were K_D = 860pM for the gold binding peptide and 19nM for the randomly selected peptide. This demonstrates that multiple phage/material interactions could take place within the same synthesis without interference.
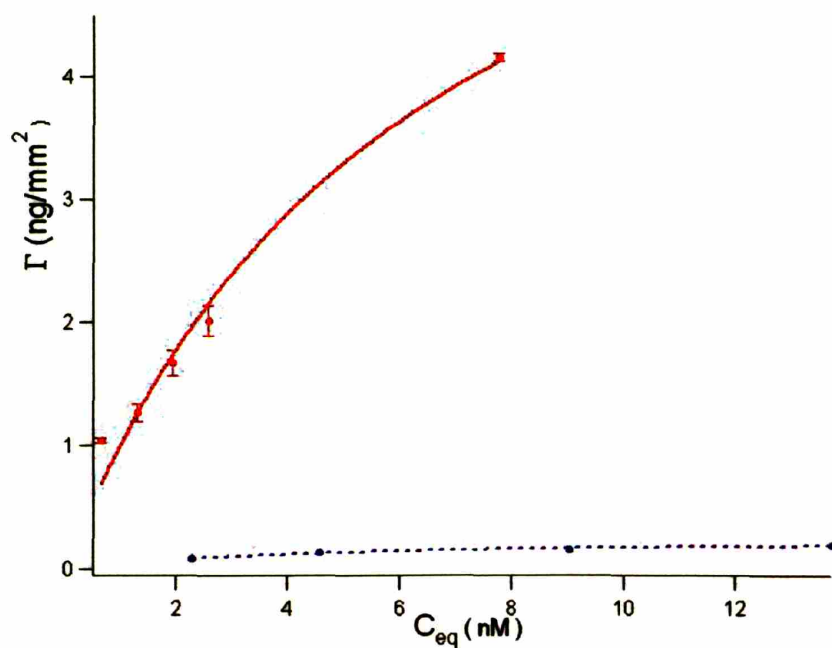
Figure 2.8 Adsorption isotherms of bacteriophage expressing the gold binding dodecapeptide (solid) and a randomly selected dodecapeptide (dashed) as a fusion to the gPIII protein on the proximal tip of the virus. Equilibrium surface concentrations were determined by SPR.

The free gold specific peptide (LKAHLPPSRLPS) was ordered for further studies from the core facilities at M.I.T., and prepared into solutions of known concentration. The free peptide was also analyzed by SPR and had a binding constant of 17uM, which is approximately four orders of magnitude less than that of the phage (figure 2.9). This is in agreement with the

fact that there are approximately three to five copies of the gPIII fusion for every phage particle. Confirmation of the binding affinity of the free peptide further validates the SPR technique as a facile route for determining the substrate affinities of gPIII fusion peptides (*23*).
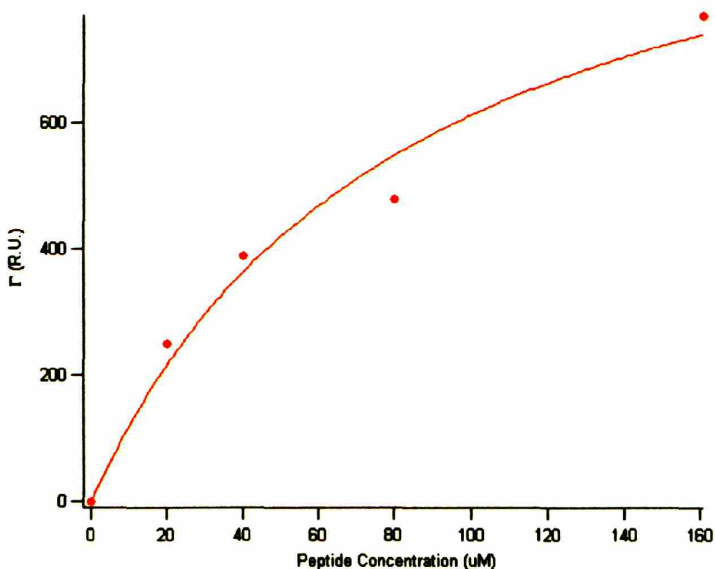

Figure 2.9 Adsorption isotherm of the Au 12-4-4 free peptide as determined by SPR.

2.5.2 *Computational Analysis*

Molecular mechanics simulations of the gold binding peptide LKAHLPPSRLPS in a 50Å^3 periodic solvent box (2014 water molecules) using the AMBER force field (Hyperchem 6.0) were run on an Athalon 2100 personal computer running at 1.7 GHz; clock times where on the order of 3-5 days. Molecular mechanics modeling of the gold specific peptide revealed that the Pro-Pro residue has a dramatic effect on the secondary structure of the peptide bringing the reactive side groups in plane with each other, providing a possible means of attachment to the gold surface (figure 2.10).
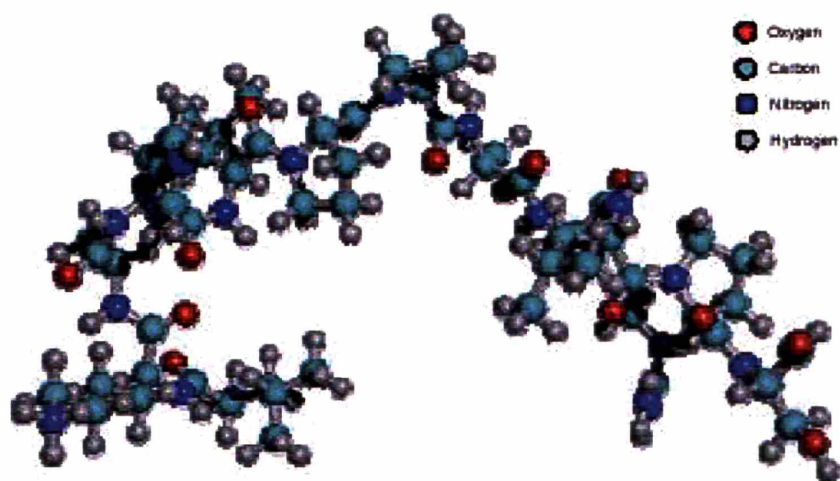
Figure 2.10 Molecular Mechanics simulation of the gold binding peptide in a periodic solvent box. The Pro-Pro residue in the center of the peptide has a dramatic effect on the overall peptide structure.

References

1. Belcher, A. M. et al. Control of Crystal Phase Switching and Orientation by Soluble Mollusc-Shell Proteins. *Nature* **381**, 56-58 (1996).

2. Falini, G., Albeck, S., Weiner, S. & Addadi, L. Control of Aragonite or Calcite Polymorphism by Mollusk Shell Macromolecules. *Science* **271**, 67-69 (1996).

3. Murray, C. B., Kagan, C. R. & Bawendi, M. G. Synthesis and Characterization of Monodisperse Nanocrystals and Close-Packed Nanocrystal Assemblies. *Annu. Rev. Mater. Sci.* **30**, 545-610 (2000).

4. Whaley, S.; English, D.; Hu, E.; Barbara, P.; Belcher, A. Selection of peptides with semiconductor binding specificity for directed nanoparticle assembly. *Nature,* **2000**, *405*, 665-668.

5. Flynn, C.E.; Lee, S.W.; Pelle, B.; Belcher, A.M. Viruses as vehicles for growth, organization and assembly of materials. *Acta Materialia* **2003**, *51*(19), pp. 5867-5880.

6. Ph.D.-12™, Ph.D.-7™, Ph.D.-C7C™ Phage Display Peptide Library Kit Instruction Manuals, *New England Biolabs.*

7. Veronese, F.M. Peptide and protein PEGylation a review of problems and solutions. *Biomaterials* **2001**, *22*(5), pp. 405-417.

8. Gooch, E.E.; Biomolecule Interactions on Calcium Carbonate and Stoichiometrically Similar Biomedical, Optical and Electronic Materials. *Graduate Thesis*, The University of Texas, Austin. **2004.**

9. Whalley, S.R.; Selection of Peptides for Binding Semiconductor and Magnetic Materials for the Purpose of Organizing Nanoscaled Materials. *Graduate Thesis*, The University of Texas, Austin, **2001**.

10. Puntes, V. F., Krishnan, K. M. & Alivisatos, A. P. Colloidal Nanocrystal Shape and Size Control: The Case of Cobalt. *Science* **291**, 2115-7 (2001).

11. Sun, S.; Murray, C. B.; Weller, D.; Folks, L.; Moser, A. Monodisperse FePt nanoparticles and Ferromagnetic FePt Nanocrystal Superlattices. *Science* **2000**, *287*, pp. 1989-1992.

12. Liou, S.H.; Huang, S.; Klimek, E.; Kirby, R.D.; Yao, Y.D. Enhancement of coersivity in nanometer-size CoPt crystallites. *J. App. Phys.* **1999**, *85*(8), pp. 4334-4336.

13. Kane, S. A. & Lippard, S. J. Photoreactivity of Platinum (II) in Cisplatin-Modified DNA Affords Specific Cross-Links to HMG Domain Proteins. *Biochemistry* **35**, 2180-2188 (1996).

14. Mooney, B. P., David, N. R., Thelen, J. J., Miernyk, J. A. & Randall, D. D. Histidine Modifying Agents Abolish Pyruvate Dehydrogenase Kinase Activity. *Biochem. Biophys. Res. Comm.* **267**, 500-503 (2000).

15. Lupinkova, L., Metz, J. G., Diner, B. A., Vass, I. & Komenda, J. Histidine Residue 252 of the Photosystem II DI Polypeptide Is Involved in a Light Cross-Linking of with the Polypeptide with the α Subunit of cytochrome b-559: Study of a Site-Directed Mutant of *Synechocystis* PCC 6803. *Biochem. Biophys. Acta* **1554**, 192-201 (2002).

16. McClelland, M. et al. Complete genome sequence of Salmonella enterica serovar Typhimurium LT2. *Nature* **413**, 852-6 (2001).

17. Parge, H. E. et al. Structure of the Fibre-Forming Protein Pilin at 2.6 A Resolution. *Nature* **378**, 32-38 (1995).

18. Kobayashi, M. & Shimizu, S. Cobalt Proteins. *Eur. J. Biochem.* **261**, 1-9 (1999).

19. Liedberg, B.; Carlson, C.; Lundstrom, I. An infrared reflection-absorption study of amino acids adsorbed on metal surfaces: l-histadine and l-phenylalanine on gold and copper. *J. Coll. Inter. Sci.*, **1987**, *120*(1), pp. 64-75.

20. Shoeib, T.; Hopkinson, A.C.; Siu, K.W.M. Collision-induced dissociation of the Ag^{+}-proline complex: Fragmentation pathways and reaction mechanislms- a synergy between experiment and theory. *J. Phys. Chem. B.*, **2001**, *105*(49), pp. 12399-12409.

21. Luey, J.; McGuire, J.; Sproull, R.D. The effect of pH and NaCl concentration on adsorption of beta-lactoglobulin at hydrophilic and hydrophobic silicon surfaces. *J. Coll. Inter. Sci.*, **1991**, *143*(2), pp. 489-500.

22. Kay, B. K., Winter, J. & McCafferty, J. (eds.) *Phage Display of Peptides and Proteins* (Academic Press, San Diego, 1996).

23. Stenburg, E.; Persson, B.; Roos, H.; Urbaniczky, C. Quantitative determination of surface concentration of protein with surface plasmon resonance using radiolabeled proteins. *J. Coll. Inter. Sci.*, **1991**, *143*(2), pp. 513-526.

CHAPTER 3

3.1 *Introduction*

The same genetic versatility of the M13 phage that makes its advantageous for use as a screening vehicle also provides the ability to develop a biological scaffold for synthesizing and organizing materials on the nanometer scale (*1*). Peptides displayed on the proximal tip of the phage (gPIII) discovered during the phage display screening of inorganic substrates can be displayed on three other proteins that make up the bacteriophage (gPVI, VII, VIII). This genetic flexibility can enable the virus with multiple functionalities based on placement and copy number of expressed peptides (*2*). The synergy between using the phage as a screening device and as a bioscaffold expedites the time in which a completely new material can be screening and implemented into functional devices.

3.2 *Display of Peptides*

3.2.1 *Proximal Tip Display*

The M13 bacteriophage used in the library has been genetically altered in their native DNA to express specific peptides which are randomly generated during transcription. Because of this, phage isolated during the selection process need no further modification in order to express functional peptides as fusions to the gPIII protein. Further, by having the peptide fusion incorporated into the complete M13 genome, expression occurs at 100% efficiency. That is, every copy of the gPIII protein on the phage particle will display a copy of the functional peptide. It should be noted that peptides not discovered through phage display can be displayed by incorporating the appropriate oligos into the M13 genome or via a phagemid system, discussed in the next section. Concentrated stock solutions of phage expressing a desired gPIII

fusion peptide are obtained by isolation of a single bacterial plaque that has experienced only a single infection event during the tittering process, followed by amplification using standard techniques (3).

3.2.2 Capsid Display

Display of functional peptides, discovered through phage display screening, as a fusion onto the gP VIII phage capsid protein was achieved using the pMoPac33 vector phagemid system constructed by Andrew Hayhurst (Gergiou Laboratory, University of Texas, Austin, ICMB). In general, a modified phage DNA plasmid (phagemid), coding for the production of the gPVIII protein, with the addition of a fusion peptide, is inserted into a bacterial host that can be infected by the M13 bacteriophage. The sequence of the fusion peptide is determined by a region of the vector that is easily changed using standard restriction and ligation procedures (4). As the modified DNA does not contain the entire phage genome, a helper phage, that does include all of the genes necessary for phage production, must be introduced into the bacterial host through an infection event. After infection with the helper phage, which begins expression of the native (or wild type) gPVIII protein, expression of the modified DNA is induced by activation of the *lacZ* gene by IPTG. This begins expression of the modified gPVIII protein that has the functional peptide fusion. During the assembly process gPV DNA sequestering proteins are replaced by the gPVIII protein as extrusion of the phage particle occurs through the cell membrane (5). Because there are now both modified and unmodified gPVIII proteins available during assembly, both will be incorporated into the phage particle. The degree to which incorporation of the modified gPVIII protein will occur is then only dependant on any

deleterious effects that the fusion peptide has on the stability of the phage capsid. These effects are typically steric and or electrostatic in nature, and thus limit the size and charge of peptides that can be fused to the gPVIII protein (*6,7*).

Specifically, the pMoPac33 vector is based on the pAK400 vector developed by Krebber et al, with the exceptions; ampicilin resistance marker; a HuCk domain for scAb (scFv-HuCk) expression; a his6-myc tag of pHEN2; a skp cistron (figure 3.1). The pMoPac33 phagemid was received from A. hayhurst in an e. coli host.
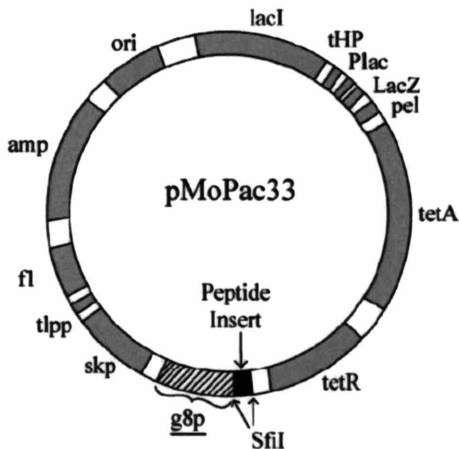
Figure 3.1 pMoPac33 vector (~6760 base pairs) used for expressing peptides as a fusion to the gPVIII capsid protein. The region in black is the peptide insert region and is flanked by gene VIII and the SFi1 restriction site.

The pMoPac33 vector was prepared for ligation with the oligos by amplifying it in its bacterial host, followed by purification using gel electrophoresis. A Qiagen DNA miniprep (QIAprep® Miniprep) kit was used for DNA purification and involved an alkaline lysis of the amplified bacteria, followed by adsorption of the pMoPac33 DNA onto a silica membrane, allowing for the thorough removal of lysate via washing. A single colony of bacteria containing the pMoPac16 vector was isolated from a bacterial lawn and amplified in LB medium at 37°C under vigorous

shaking for ~12 hours. The cells were collected by centrifugation at 10,000 rpm at 4°C for 10 minutes. The bacteria are then lysed using an alkaline buffer followed by neutralization, and adjustment of the DNA containing solution to high-salt binding conditions using the appropriate buffers provided in the kit. Isolation of the DNA from the lysate was carried out using the QIAprep silica membrane. DNA selectively binds to the membranes under high-salt conditions. After immobilization of the DNA onto the membranes, lysate is removed by washing of the membrane with a guanidine hydrochloride / isopropanol containing buffer. Elution of the DNA is achieved by reducing the salt concentration of the solution, typically by incubation of the membrane in type 1 water adjusted to a pH of 7.5; maximum elution efficiency is achieved in the pH range 7.0-8.5, according to the QIAprep handbook (8). The isolated DNA was prepared for ligation by reaction with the SfiI restriction enzyme. 20uL of the mini prep DNA was added to 5uL NE Buffer 2; 0.5uL BSA; 1uL SfiI; and water to a final volume of 50uL. This was incubated at 50°C for four hours. After the restriction digest, gel electrophoresis was used to verify the SfiI/DNA interaction and to isolate the desired DNA fragment. 10uL of the digest product was mixed with equal amounts of gel loading buffer and run on a 1% agarose (ethidium bromide) gel at 120V for ~30min (will vary and should be monitored closely during the first attempt to gage running time.) A 1kb DNA ladder was also loaded into the gels as a marker for determining the molecular weights of the isolated digest products.   The DNA band at approximately 4700kb was cut from the gel using a uv light box for visualization. A gel extraction kit (Qiagen) was used to separate the DNA from the agarose gel by dissolution of the gel using the QC buffer, followed by isopropanol induced precipitation of the DNA. The DNA precipitate was collected by centrifugation of the solution through a membrane. A wash fluid

was placed above the membrane and centrifuged through to remove any residue from the DNA. After washing, the DNA was eluted from the membrane using the appropriate buffer provided.

Appropriate oligos were ordered that encoded for the desired peptide fusion, and followed the form of...

$$5' - CGGCCATGGCG \_\_\_ \_\_\_ \_\_\_...\_\_\_ TCGG - 3'$$

$$3' - TCGGCCGGTACCGC\_\_\_ \_\_\_ \_\_\_...\_\_\_ A - 5'$$
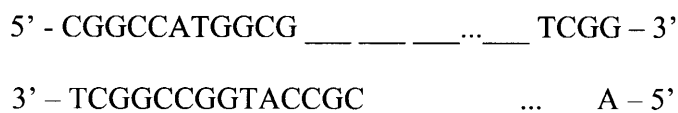
where the underlined spaces represent the standard genetic code of the amino acids in the fusion peptide. Preparations of the oligos for ligation into the prepared DNA discussed above involved the preparation of 50pM/uL solutions in TBS. The oligos solution was then annealed in ligation buffer at 80°C for 5 minutes, followed by cooling to room temperature. Ligation proceeded by reaction of the annealed oligos with the gel purified DNA in ATP containing ligation buffer, and was initiated by the addition of T4 DNA ligase; ATP is a co-enzyme to the T4 DNA ligase, and is necessary for ligation to occur. Transformation of the plasimid into the e. coli host was achieved using competent cells, either electro or chemical (Ca^{2+}), which were grown from a glycerol stock solution stored at -80°C. Cells that have not been cryogenically stored have greater transformation efficiency, and should always be prepared immediately prior to transformation. Ligated plasmid containing the oligo insert, along with ligated plasmid not containing an insert and non-digested pMopac16 plasmid (as negative and positive controls, respectively) were spread onto ampicilin containing agarose plates and incubated overnight at 37°C. Digestion of the amplified plasimid and negative control plasmid is performed for gel electrophoresis analysis of the two systems. The bands in the two systems should be identical

with the exception of the insert size. Sequencing of the DNA using the AHX167 primer (5' –

GCCTACGGCAGCCGCTGG – 3' confirmed the presence of the oligos.

Amplification –

Amplification of the modified gPVIII phagemid bacteria was carried out by selection of a

single colony from the ampicilin plates and incubating it with 50mL of LB media at 37°C for 12

hours under vigorous shaking; this is referred to as an overnight culture (OC). A 100-fold

dilution of the OC into cell growth media is prepared and incubated at 37°C for approximately

two hours under vigorous shaking (300-500 RPM), or until the solution has reached the mid-log

phase. Infection of the culture with helper phage at the optimum infection ratio of cells to phage

(5:1) is followed by incubation without shaking for 45 minutes. The infection process is allowed

to occur at 37°C without shaking, to prevent shearing of the phage particle in the cell wall due to

the forces generated by the shaking. After the initial infection event has occurred, chemical

induction of the phagemid is achieved by addition of 100uM/uL of IPTG. The culture is then

allowed to grow at 37°C under vigorous shaking for four to six hours. For large scale

amplification (volumes greater than 500mL) one can use either LB or Glucose containing terrific

broth (TB). Terrific broth supports greater cell densities, producing a higher yield of phage, but

the phage seem to have a lower expression of the modified peptide than when grown in LB. The

choice of growth media is then determined by the end application of the phage. For solution

based applications (such as mineralization.) the use of TB is advantageous, as it produces a

greater overall number of functional peptides. If it is imperative that each phage have a high

expression number of functional peptides, than it is suggested that LB be used as the cell growth

medium.

Isolation of the amplified phage is achieved by removal of the e. coli by centrifugation at 10,000 rpm (4°C) for 15 minutes. This process is repeated and the upper 80% of the supernatant is collected for further purification of the phage. Addition of 1/6 by volume of 20% PEG-NaCl at 4°C for 12 hours induces precipitation of the phage. The phage is then removed from solution by centrifugation (10,000rpm, 4°C, 10 min.) and resuspended in TBS. This process is repeated, with the exception that the phage precipitation occurs at 0°C for two hours. After resuspension of the phage pellet into TBS, an equal amount of chloroform is added to remove any residual cell lysate and to further purify the phage stock. Separation of the two phases is completed by centrifugation at low speeds (300-500 rpm) for five minutes. Removal of the aqueous phase without disturbance of the chloroform layer results in a clean phage stock; failure to fully remove e. coli cells and cell lysate dramatically reduces the shelf life of amplified phage stocks. Although it is imperative for phage viability that they be stored, in the short term, in TBS pH 7.5 at 4°C, the high salt concentration of the TBS often interferes with the experiments discussed in later chapters. Therefore, dialysis of the amplified phage stock against 4L of type 1 water using 15mL dialysis cassettes (promega) was performed for 4 hours with the water being changed out every hour. Complete removal of the TBS buffer results in the precipitation of the phage, which is reversible under addition of TBS. Phage stocks can be stored for long periods at -20°C.

3.2.3 *Distal Display*

Expression of the gold binding peptide as a fusion to the gPIX protein on the distal tip of the phage particle was achieved using a similar phagemid system as discussed above. Although this was done to provide a tri functional phage for device assembly, it was determined through experiment that having only one terminus of the phage binding to the substrate was preferable

for flow alignment. Also, multiple functionalities for the same substrate caused fouling of the surface with phage through non-specific matting.

3.2.4 *Multifunctional Display*

The utilization of multiple components of the M13 bacteriophage is achievable by combining the two strategies for expressing fusion peptides discussed above. To achieve bi- and tri-functional phage, a gPVIII phagemid system is infected with a library selected helper phage. Because the gPIII fusion is incorporated into the full genome provided by the helper phage. It will be expressed with 100% efficiency and occurs without any further modification to the system. Introduction of the phagemid into the host cell then allows for the incorporation of modified gPVIII proteins into the capsid of the modified gPIII phage. This system can be further extended to include functional peptide fusions to the proximal (gPIII), distal (gPVII) and capsid (gPVIII) by incorporating both the gpVIII and gPVII genes into the phagemid system. This was performed for the gold system and for the CoPt system yielding phage whose distal tip displayed the gold specific peptide LKAHLPPSRLPS and whose capsid displayed either the gold specific or CoPt specific peptide. The functionality of the proximal tip was then determined by the helper phage used.

3.3 *Modeling of displayed peptides*

gPVIII incorporation Density-

Computational analysis was performed with help from Stephen Kottmann to obtain a clear image of the modified capsid system in which a fusion peptide is randomly incorporated during phage assembly. Incorporation of modified gPVIII monomers during phage assembly is highly

dependant on the size and charge of the fusion peptide expressed. Therefore it is necessary to determine a minimum incorporation percentage that will yield a phage capsid with sufficient functional peptide expression so as to act as a usable bioscaffold. In order to obtain a qualitative figure of minimum incorporation, the phage capsid was constructed with the random incorporation of the modified gPVIII monomer and analyzed for fusion peptide density. All structural data of the wild type capsid was obtained from the Protein Data Bank (PDB) file #1ifj, authored by D.A. Marvin et al. In summary, fiber diffraction data on the filamentous bacteriophage was obtained at a resolution of 3.3A. Hyperchem 6.0 was used to add the A7 ZnS specific constrained heptapeptide to the gPVIII monomer as obtained from the PDB file followed by energy minimization of the fusion peptide using the Fletcher-Reeves conjugate gradient optimization algorithm. Because the gPVIII monomer structure was determined via x-ray crystallography, it was not allowed to move during the energy minimization, but was present in the calculations. The capsid was then reconstructed from the PDB data with the modified gPVIII monomer unit added to the assembly matrix using a random number generator set to predetermined incorporation percentage. The fusion peptide density was then calculated for incorporation percentages between zero and one hundred. The density followed a linear trend similar to that obtained from a 1-D test system. However, according to this method, the fusion peptide nearest neighbor separation levels off at approximately 3.0nm at and above 20% incorporation (figure 3.2). Consequently, high incorporation of the substrate specific fusion peptides is not required for complete mineralization of the virus to occur.
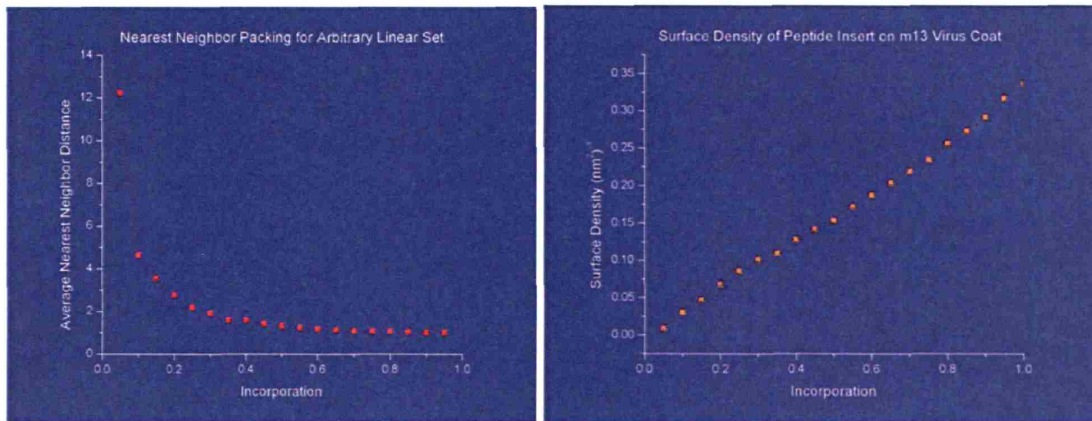
Figure 3.2 Nearest neighbor distance for gPVIII fusion peptides as a function of expression efficiency (left). Surface density of the gPVIII fusion peptide as a function of expression efficiency (right).

Peptide Stability –

During assembly, stacking of the gP8 unit cell results in a five-fold symmetry down the length (c-axis) of the virus (figure 3.3) and is the origin of the ordering of fusion peptides in a three-dimensional structure (figure 3.4). To exam whether or not the symmetry of the phage capsid is imparted to the fusion peptide, monte carlo calculation of a model peptide system was performed.
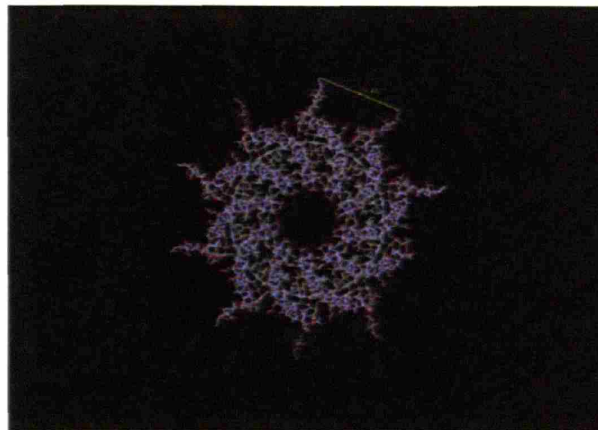
Figure 3.3 Visualization of the phage capsid expressing a 7c peptide as a fusion to the gPVIII protein along the c-axis of the virus.
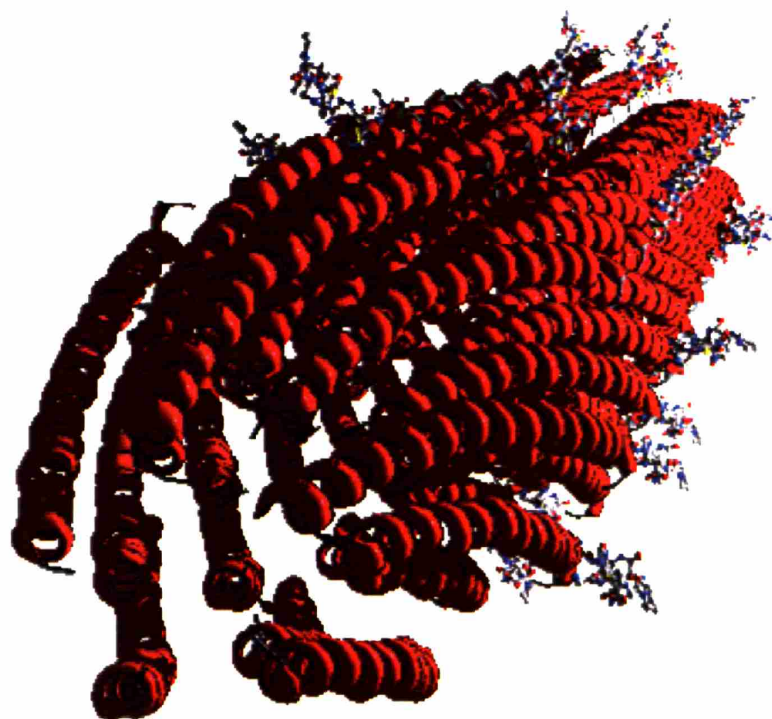
Figure 3.4 Visualization of the fusion peptide on the gPVIII capsid. Image represents a 20% expression efficiency.

The A7 constrained heptapeptide was chosen for simulation and the overall dihedral angle was calculated for the free unconstrained peptide; the disulphide constrained peptide; the disulphide constrained peptide in a capsid segment after 1 million steps. The peptide inserts were modeled in the capsid environment using Monte Carlo software MCPRO (Jorgensen, W.L., MCPRO, Version 1.68, Yale University, New Haven, CT, 2002.) with solvent effects accounted for by the Poisson-Boltzmann toolkit ZAP (OpenEye Scientific Software.) The values obtained for the overall dihedral angle of the peptides were 27.269, 18.103, and 14.267 respectively and are visualized in figure 3.5.
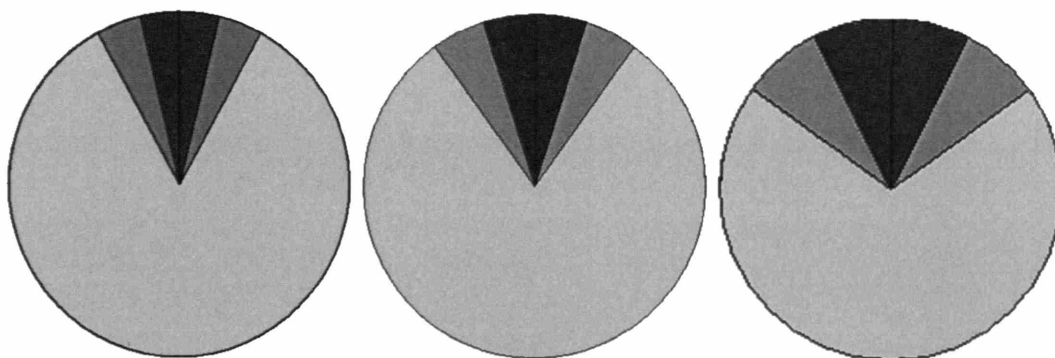
Figure 3.5 Representations of the dihedral angle of the A7 constrained heptamer peptide as a Free peptide (right) constrained peptide (center) and as expressed in the capsid of the M13 bacteriophage. The darkest region represents +/- σ, and the area covered by the medium dark color represents an angle of +/- 2σ.

3.5 *Discussion*

The dramatic decrease of the overall dihedral angle of the A7 constrained peptide demonstrates that the peptide influences steric effects when inserted into the capsid. This is an important aspect of the M13 bacteriophage as a bioscaffold. By being able to display peptides along the capsid in a uniformly oriented manner, a rigid, reproducible template can be easily synthesized through bacterial amplification. The multiple display regions, and the possibility of incorporating functional peptides into proteins not in the phage assembly, but encoded for by the M13 genome provide multiple pathways for exploring biomineralization.

References

1. Malik, P; Perham, R.N. Simultaneous display of different peptides on the surface of filamentous bacteriophage. *Nuc. Acids. Re.* **1997**, *25*(4), pp. 915-916.

2. Smith, G.P. Surface display and peptide libraries. *Gene* **1993**, *128*, pp. 1-2.

3. Sambrook, J., Fritsch; E. F.; Maniatis, T. *Molecular Cloning: A Laboratory Manual* (Cold Spring Harbor Laboratory Press, Cold Spring Harbor, NY, **1990**).

4. Kay, B. K.; Winter, J.; McCafferty, J. (eds.) *Phage Display of Peptides and Proteins* (Academic Press, San Diego, **1996**).

5. Horn, N. Isolation of high affinity ligands against SH3 and EVH1 domains using the phage display cosmix-plexing technology. *Doctorate Thesis*, The Technical University of Carolo-Wilhelmina at Braunschweig, Germany, **2000.**

6. Wilson, D.R.; Finlay, B.B. Phage display: applications, innovations, and issues in phage and host biology. *Can. J. Microbiol.* **1998**, *44*(4), pp. 313-329.

7. Malik, P. et. al. Role of capsid structure and membrane protein processing in determining the size and copy number of peptides displayed on the major coat protein of filamentous bacteriophage. *J. Mol. Bio.* **1996**, *260*, pp. 9-21.

8. QIAprep miniprep handbook, Second Edition. QIAgen Inc. June **2005**.

4.1 *Introduction*

Biological organisms have evolved the ability to control the synthesis and assembly of inorganic materials through proteins under environmentally benign conditions. Several examples exist in nature of protein-mediated inorganic synthesis, and researchers have begun manipulating these organisms and proteins to synthesize inorganic materials with controlled composition and crystallinity. Examples include the use of viruses expressing material-specific peptides to nucleate semiconducting nanoparticles(*1,2*), modification of the iron storage protein ferritin (*3*), manipulation of bacteria and yeast to produce semiconducting materials (*4*), and metal-specific polypeptides selected from combinatorial libraries (*5*). Biological factors have also been used to assemble nanoscale materials into heterostructures using self-assembly motifs commonly found in nature (*6*).

Here we use biological templating as a synthetic scheme to nucleate and organize nanoparticles of technologically important materials. This biologically based synthetic strategy has several advantages over more recent chemical synthetic methods including the direct synthesis of the desired magnetic crystalline phase and synthesis of the magnetic materials under ambient temperature, pressure, and atmosphere (*7*). In addition the viral system employed uses bacterial amplification of the "organic" templates, making their synthesis easy and cost effective.

4.2 *Methods and Materials*

All peptide driven materials synthesis involved incubation of the peptide template with aqueous metal salts. For semiconducting materials, precursors were added sequentially and included; $CdCl_2$; $ZnCl_2$; NaS. For the magnetic materials studied, $CdCl_2$; $FeCl_2$; H_2PtCl_6 were used as the precursors and were added simultaneously in the case of the alloy systems CoPt and

FePt. Metallic and magnetic materials required the chemical reduction of the ionic precursors into their zero valent state. Sodium borohydride (NaBH$_4$) was used at or bellow 50mM concentrations. Above 100mM, phage are no longer stable and loose their ability to infect, which is taken as a sign of disassembly of the capsid.

In the case of FePt 1 ml of phage displaying the functional dodecapeptide on the proximal tip (10^{12} phage/ml) was mixed with 5 ml of 0.01mM FeCl$_2$ and 5 ml of 0.01 mM H$_2$PtCl$_6$. This mixture was vortexed for ten minutes to ensure mixing, and 5 ml of 0.05 M NaBH$_4$ was added to reduce the metals forming the desired nanoparticles. Nanoparticles of CoPt and Co were prepared similarly by substituting the corresponding metal salts at similar concentrations.

Particle nucleation using the synthetic peptide was accomplished by substituting 100 ml of synthetic peptide (Sigma-Genosys) at a concentration of 10 mg/ml. Particles were precipitated from solution by pegylation (addition of 5 ml of 20% PEG-NaCl solution (w/v), followed by incubating at 4 C for 60 minutes.) Following precipitation, the solution was centrifuged at 10,000 g for 10 minutes. The black pellet was resuspended in 1 ml of H$_2$O for further analysis.

CoPt wires were synthesized by the interaction of 1mL of CoPt specific viruses (10^{12} phage/mL) with 0.5mM CoCl$_2$ and 0.5mM H$_2$PtCl$_6$ in a 1:1 ratio at 0°C overnight. In the case of FePt 1 ml of phage (10^{12} phage/ml) was mixed with 0.01 mM FeCl$_2$ and 0.01 mM H$_2$PtCl$_6$. These mixtures were vortexed for ten minutes to ensure proper mixing, and 0.1 M NaBH$_4$ was added to reduce the metals forming the desired nanoparticles. The solution was allowed to rest for at least two hours to let the reaction go to completion as any unreacted NaBH$_4$ will react with the TEM grid causing it to foul. The CoPt and FePt systems were applied directly to SiO TEM

grids. Annealing of the samples was performed under forming gas (5% H_2) to prevent the onset of oxidation for 3 hours at $350°$ C with a ramp rate of $5°C/min.$ using a Thermolyne tube furnace.

Thermal gravimetric analysis was performed on the Perkin Elmer 200 TGA/DTA, with flow gasses consisting of air, argon, and forming gas (5% H_2). Samples were prepared by centrifugation of the virus-particle suspension into 1mg pellets and allowed to dry. TEM Thermal analysis of the CoPt system was performed in situ on the JEOL 200CX microscope operated at 200 kV, using a Gatan heat stage.

For TEM analysis, nanoparticles were imaged using a JEOL 200CX, JEOL 2010, or JEOL 2010F TEM microscope. To image and map the nanoparticle wires, the JEOL 2010F was operated under HAADF STEM mode along with energy dispersive x-ray spectroscopy (EDS) compositional mapping. Annealing of the TEM samples for analysis required the use of reinforced TEM grids (200A of SiO coated with 100A of amorphous carbon), that have had the formvar support layer removed.

For XRD measurements the concentrated particle solutions were dialyzed into 18 MOhm H_2O. Following dialysis, the nanoparticles were drop-coated onto Si wafers and analyzed using a Rigaku RU300 diffractometer. For SQUID measurements, the concentrated samples were dried to a black powder and analyzed using a Quantum Design DC SQUID.

4.3 *Nucleation*

The peptides selected in these experiments that bind specifically to metallic, magnetic and semiconducting materials are able to exhibit control over the crystallization of nanostructures (*8*). Three functional peptide systems were developed for studying the ability of said peptides to control the shape, size, composition and morphology of nanoscaled materials and include; gPIII fusion systems; free peptides; gPVIII fusion systems. Because the functional peptide discovered during phage display is already encoded in the genome of the isolated phage, amplification of the selected clone is the most economical and easily producible means of generating the desired peptide in large quantities. However, non-specific interactions of the capsid during materials synthesis produced materials with greater defects and without control over their physical properties. Because of this, functional peptides were synthesized using standard peptide chemistry and used in subsequent studies.

Utilizing the linear form and high aspect ratio of the capsid is a natural direction for both nucleating and organizing material on the nanoscale (*9*). Expression of functional peptides as a fusion to the gPVIII capsid protein was achieved using a phagmid system (*10*). Expression efficiencies greater than 20% yielded phage-based bioscaffolds that could be completely mineralized. The high crystallinity of the capsid imparts directional ordering of the peptide fusion (*11*). This ordering is also imparted to the nucleated material and promotes preferential crystallographic ordering of the nucleated material with respect to the c-axis of the phage. Removal of the organic scaffold via thermal annealing then promotes single crystal growth through a preferred orientation aggregation based mechanism (*12*), resulting in free standing inorganic nanowires.

4.3.1 *Proximal Tip Nucleation*

Low and high resolution transmission electron microscopy (TEM) images of FePt and CoPt nanoparticles prepared using the gPIII modified phage confirm the room temperature synthesis of the $L1_0$ phase of these materials (figure 4.1).
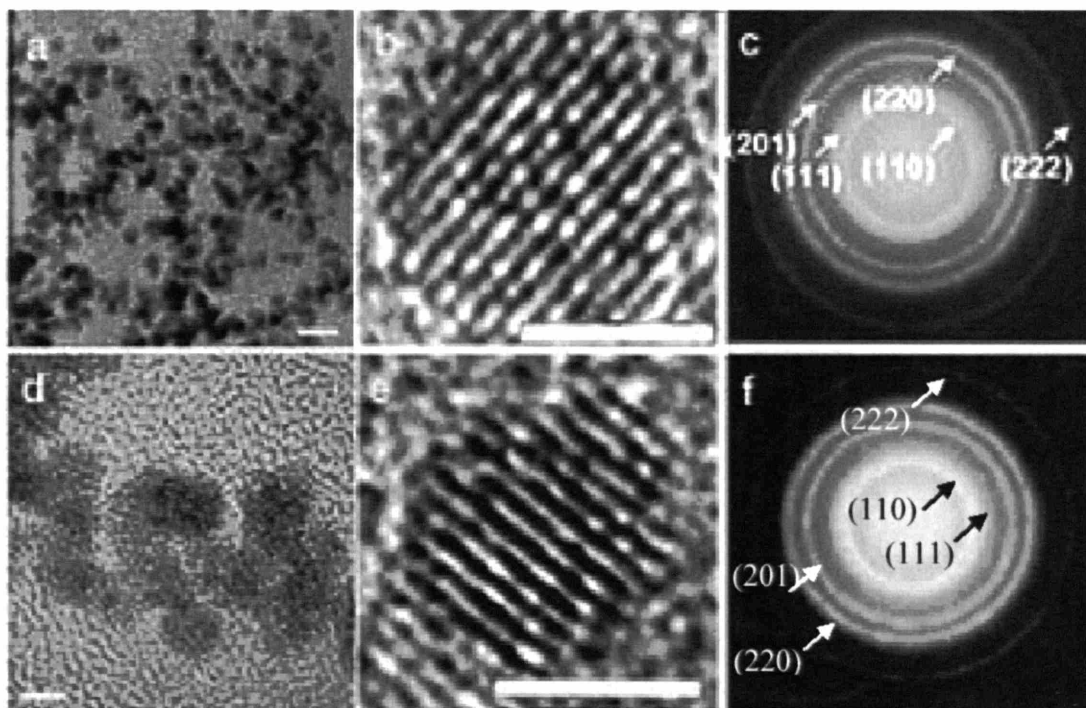

Figure 4.1 Nucleation of FePt (top) and CoPt (bottom) nanoparticles using functional peptides displayed on the gPIII protein located on the proximal tip of the phage particle. Low resolution (a,d) and High reolution (b,e) TEM was used to image the particles. Electron diffraction patterns (c,f) confirmed the presence of the L10 phase.

The lattice spacing in the image of the FePt particle is 0.22 nm, which is in good agreement with the literature value of 0.219 nm for the (111) facet of $L1_0$ FePt (PcDF # 65-1051). The lattice spacing of the CoPt nanoparticle in this image is 0.27 nm, and is good agreement with the value of 0.269 nm for the (110) facet of CoPt (PDF # 3-1358). Additionally, the selected area electron diffraction pattern (Figure 1c) indicates these nanoparticles are composed of $L1_0$ FePt. The rings corresponding to the (110), (111), (201), (220) and (222) facets are labeled and the (110) and (220) are especially indicative of $L1_0$ FePt. Previous

experiments with FePt nanoparticles have demonstrated that the (110) band is not present in films prepared from preannealed, disordered FePt nanoparticles (*13,14*), and its presence here suggests the nanoparticles are nucleated as the $L1_0$ phase of FePt. The selected area electron diffraction pattern of these nanoparticles also confirms the presence of the $L1_0$ phase of CoPt, and the reflection rings can be assigned to the same facets as the $L1_0$ FePt.

The proximal tip directed synthesis of these materials also exhibited relatively good control over particle size. The FePt nanoparticles have an average diameter of 4.0 $\pm$ 0.6 nm, which is above the theoretical limit for sustaining a magnetic moment. The minimum size of FePt nanoparticle that can act as a ferromagnet at room temperature is 2.8 nm (*15*). The CoPt nanoparticles have an average diameter of 3.5 $\pm$ 0.7 nm. Only non-crystalline and polycrystalline nanoparticles could be found in control experiments involving phage that express a random peptide, wild-type phage that do not express any insert, and no phage.

The magnetic properties of the nucleated nanoparticles were characterized using vibrating sample magnetometry (VSM) and super conducting quantum interference device magnetometry (SQUID). To accomplish this, the as-prepared FePt nanoparticles were pressed into a pellet and characterized using a Quantum Design dc-SQUID magnetometer. The hysteresis loop taken at 300 K shown in Figure 4.2 shows the nanoparticles have a high saturation magnetization (Ms) and a small amount of coercivity (10 Oe). To determine the cause of the low coercivity, Ms vs T measurements were taken. Ms initially decreases quite rapidly with temperature. One possible explanation for the behavior is the existent of a low Curie temperature phase. However, the composition of such a phase is currently not clear. The initial reduction in Ms with temperature is followed by a more gradual decrease for T>20K, and attempts to model this more gradual decrease in Ms using the Brillouin function lead to a rather poor fit.
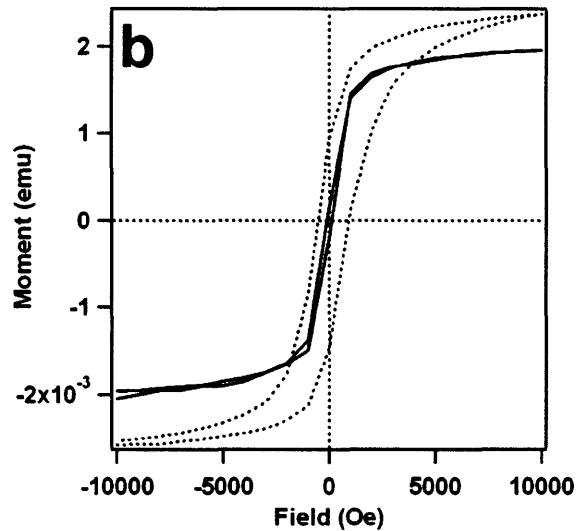
Figure 4.2 SQUID analysis of the FePt particles synthesized by the FePt specific peptide displayed on the proximal tip of the phage particle.

4.3.2 *Free peptide Nucleation*

The less than optimal magnetic conditions and presence of non-$L1_0$ FePt particles is believed to be caused by the relatively low concentration of FePt-specific peptide in solution since the peptide is expressed in low numbers at the proximal tip of the M13 bacteriaphage (*16*).

To investigate the effect of peptide concentration on nanoparticle nucleation, the FePt-specific dodecapeptide was prepared synthetically. Figure 4.3a is a TEM image of the subsequent nanoparticles. These nanoparticles have an average diameter of 4.1 $\pm$ 0.6 nm, and high resolution imaging (figure 4.3) shows the presence of lattice fringes. The spacing of the fringes is 0.22 nm, which corresponds with the literature value of 0.2197 nm for the (111) facet of $L1_0$ FePt. Figure 4.3c is an x-ray diffraction spectrum of these samples, showing the (110), (111), (200), (202), and (112) peaks of $L1_0$ FePt (additional peaks in the spectrum correspond to residual NaCl). The x-ray data indicates that these nanoparticles truly are composed of $L1_0$ FePt. SQUID characterization at 300K (figure 4.3e) indicates that these nanoparticles are

ferromagnetic at room temperature, possessing a coercivity of 300 Oe. This value of coercivity is much higher than the coercivity found for as-prepared FePt nanoparticles synthesised using a solution chemistry approach , which only become ferromagnetic at room temperature after annealing (*13,17*). The nanoparticles prepared using biological templates do not require subsequent annealing to achieve the desired ferromagnetic properties and this synthetic approach represents the first synthetic strategy for preparing $L1_0$ FePt nanoparticles that are dispersed in solution rather than immobilized on a substrate. This new approach can be used to prepare $L1_0$ nanoparticles at room temperature, achieving the face-centered tetragonal structure, which is typically only thermodynamically possible above 500 °C. In addition, these experiments show the ability of genetically engineered bacteriophage to bind a non-biologically prepared surface grown under non-aqueous conditions and template that same material under biological conditions.
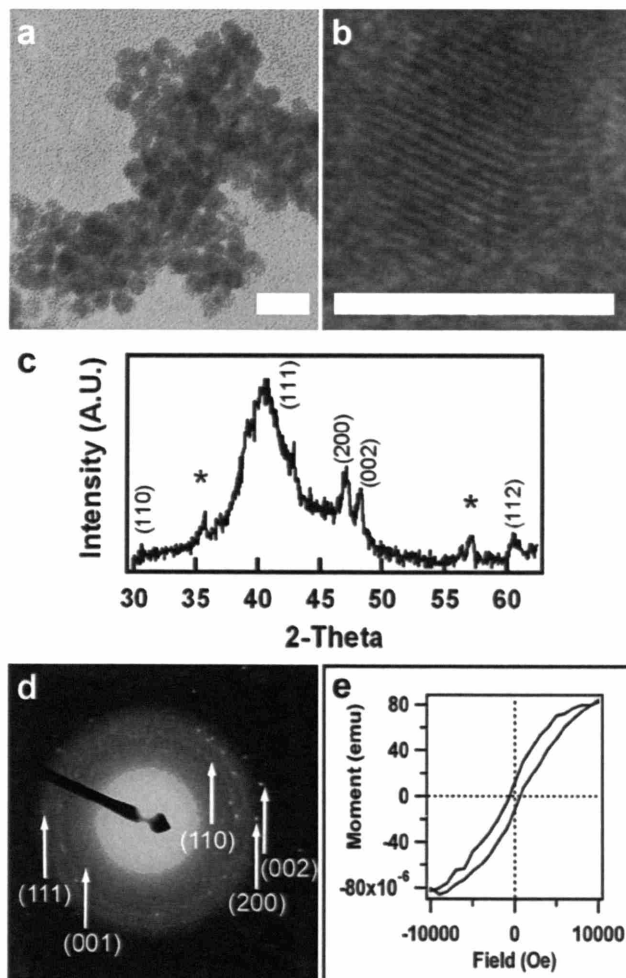
Figure 4.3 Low (a) and high (b) resolution images of FePt nanoparticles grown using synthetically prepared FePt specific dodecapeptide as a template with diffraction characterization, including X-ray diffraction (c) and selected area electron diffraction (d). SQUID characterization of similar particles (e) taken at 300 K, and 1 *Ì*m _ 1 *Ì*m

4.3.3 *Capsid Nucleation*

All of the nanoparticles described above were prepared using phage that express the peptide of interest on their P3 protein, a protein expressed on one end of their linear coat structure, or with the free synthetic peptide. To achieve higher density nanoparticle synthesis, the CoPt-specific peptide was expressed on the gPVIII protein of the phage, since the main body of the wild-type phage is composed of 2700 copies of the gPVIII protein. This also provided a linear template for organizing the nanoparticles.

The general synthesis of 1-D nanostructures based on a genetically modified virus scaffold for the directed growth and assembly of crystalline nanoparticles into 1-D arrays, followed by annealing of the virus-particle assemblies into high aspect ratio, crystalline nanowires through oriented, aggregation-based crystal growth (*18*). The synthesis of analogous nanowire structures from fundamentally different materials, the II-VI semiconductors ZnS and CdS and the $L1_0$ ferromagnetic alloys CoPt and FePt, demonstrates both the generality of the virus scaffold and the ability to precisely control material characteristics through genetic modification. In contrast to other synthetic methods, this approach allows for the genetic control of crystalline semiconducting, metallic, oxide, and magnetic materials with a universal template.

Incorporation of these peptides into the highly ordered, self assembled capsid of the M13 bacteriophage virus provides a linear template that can simultaneously control particle phase and composition, while maintaining an ease of material adaptability through genetic tuning of the basic protein building blocks.

Mineralization of the ZnS and CdS systems have been described previously (*1,10*) and involved incubation of the viral template with metal salt precursors at reduced temperatures to promote uniform orientation of the peptide molecules during nucleation (*19*), leading to the preferred crystallographic orientation of nucleated nanocrystals. Prior to annealing, wurtzite ZnS and CdS nanocrystals (3-5nm) grown on the virus surface were in close contact and preferentially oriented with the [001] direction and the (100) (ZnS) and (001) (CdS) planes perpendicular to the wire length direction, and is supported by electron diffraction, high resolution transmission electron microscopy (HRTEM), high angle annular dark-field scanning transmission electron microscopy (HAADF-STEM), and dark-field diffraction-contrast imaging (figure 4.4). Particles attached to the virus were prohibited from fusing under initial synthesis

conditions due to the blocking effects of the nucleating peptides, and therefore required removal of the template in order to form single crystal nanowires.

Electron microscopy of both the pre- and post-annealed ZnS and CdS viral nanowires confirmed the preferential orderin prior to annealing and the retention of the crystallographic direction after annealing. Dark-field Diffraction-contrast imaging of the pre-annealed ZnS system using the (100) reflection reveals the crystallographic ordering of the nucleated nanocrystals, were contrast stems from satisfying the (100) Bragg diffraction condition. The ED pattern of the polycrystalline pre-annealed wire shows the wurtzite crystal structure and the single crystal type [001] zone axis pattern, suggesting a strong [001] zone axis preferred orientation of the nanocrystals on the viral template (figure 4.5a). Bright-field TEM image of an individual ZnS nanowire formed after annealing confirms that the synthetic strategy can yield single crystal nanowires. ED pattern along the [001] zone axis shows a single crystal wurtzite structure of the annealed ZnS nanowire (figure 4.4b).
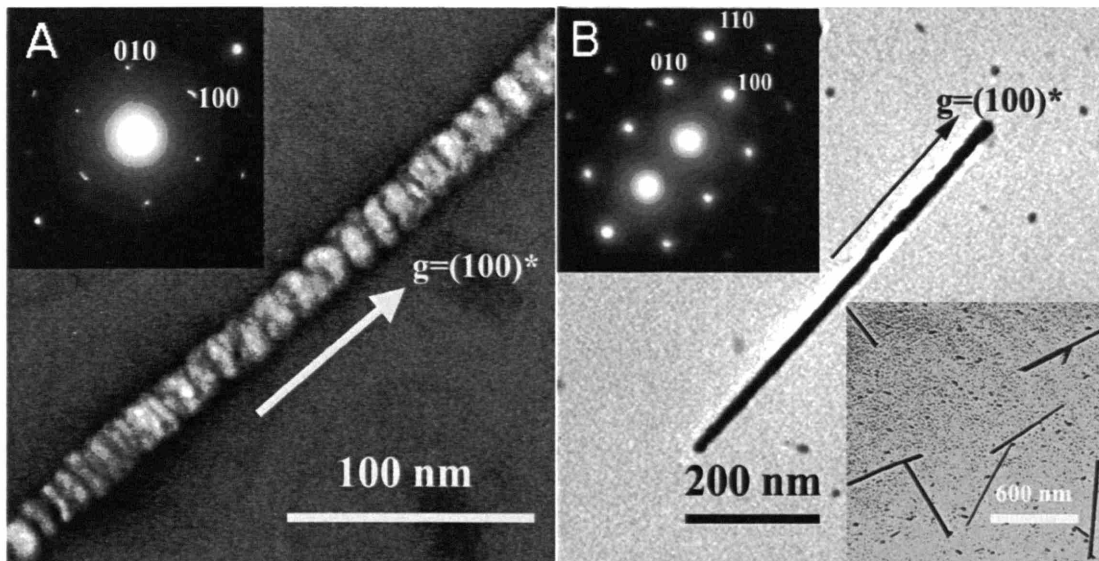
Figure 4.4 ZnS nanoparticle-phage assemblies before (left) and after (right) annealing. (a) Dark-field image showing the preferential alignment of the nanocrystals with respect to their crystallographic orientation. Insets show ED patterns of the wurtzite structure.

High Resolution TEM (HRTEM) of a ZnS single crystal nanowire shows a lattice image that continually extends the length of the wire, further confirming the single crystal nature of the annealed nanowire (figure 4.5). The measured lattice spacing of 0.33 nm corresponds to the (010) planes in wurtzite ZnS crystals. A 30° orientation of (010) lattice planes with respect to the nanowire axis is consistent with the (100) growth direction determined by ED. Synthesis of CdS wires also yielded single crystal wires confirmed by the HRTEM lattice image of an individual CdS nanowire. The experimental lattice fringe spacing, 0.24 nm, is consistent with the unique 0.24519 nm separation between two (102) planes in bulk wurtzite CdS crystals.
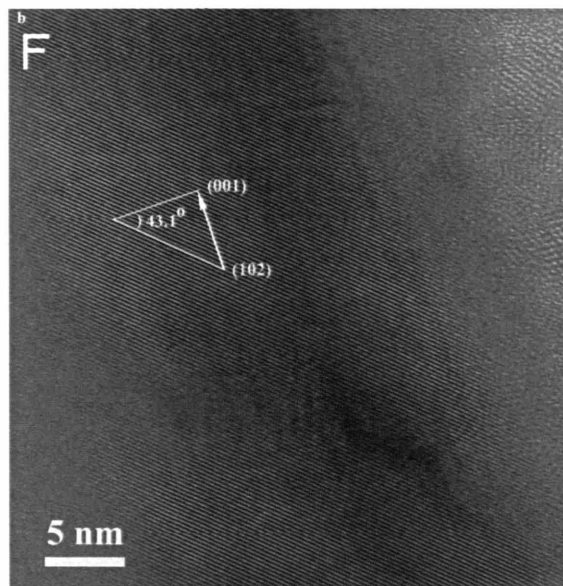
Figure 4.5 High Resolution TEM of the CdS annealed nanowires.

Annealing of the mineralized viruses at temperatures below the ZnS and CdS particle melting point (400-500° C) allowed the polycrystalline assemblies to form single crystal nanowires through removal of the organic template and minimization of the interfacial energy (*20*). Electron diffraction and HRTEM revealed the single crystal nature of individual nanowires that inherited the preferred orientation seen in the precursor polycrystalline wires through removal of the grain boundaries (figure 4.6, *21,22*). The [100] direction and (001) plane

orientations of the observed ZnS nanowires were consistent with common elongation directions for II-VI nanowires, even though these are thermodynamically high energy planes (12,18,23). HRTEM of the single crystal CdS nanowires revealed a lattice spacing of 2.4 Å that was consistent with the unique 2.4519 Å separation between two (102) planes in bulk wurtzite CdS crystals (JCPDS #41-1049). The 43.1° orientation of (102) lattice planes with respect to the nanowire axis indicated that the nanowire was elongated along the [001] direction and again confirmed the wurtzite structure.

Extending the virus-directed synthesis approach to the ferromagnetic $L1_0$ CoPt and FePt systems was a natural direction for demonstrating both the diversity of applicable materials and to address current technological issues regarding the development of low-dimensional magnetic materials. Platinum alloyed magnetic materials of the chemically ordered $L1_0$ phase have been of recent interest due to their high coercivity, resistance to oxidation, and inherent magnetic anisotropy necessary for ultrahigh density recording media (24). Although synthetic routes such as VLS yield exquisite 1-D semiconducting structures and non-specific template schemes are applicable to a range of materials, both have faced difficulties in producing high-quality, crystalline, metallic and magnetic nanowires in free standing form (25).

The M13 bacteriophage was modified by fusing either the CP7 CoPt specific or FP12 FePt specific peptide into the virus capsid. Nucleation of the CoPt and FePt particles was achieved via the chemical reduction of metal precursor salts in the presence of gPVIII modified phage. CoPt wires as synthesized by the modified virus template were soluble in water and reduction of Co and Pt salts without the presence of the virus yielded large precipitates which immediately fell out of solution (figure 4.6). TEM images of the unannealed CoPt nanoparticle-

virus system showed a mesh like structure, believed to be caused by the magnetic interactions
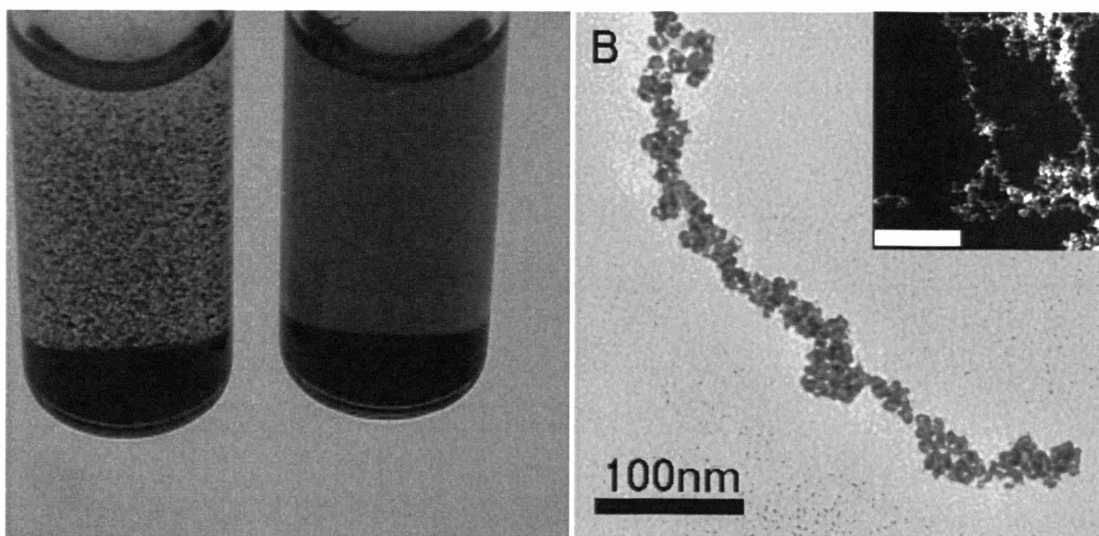
between particles (figure 4.7).

Figure 4.7 CoPt nanowire synthesis with (right) and without (left) phage (a). Low resolution TEM image of crystalline $L1_0$ CoPt wires (~650nm x 20nm), insert shows STEM image of the unannealed CoPt wires. Both scale bars shown are 100nm.
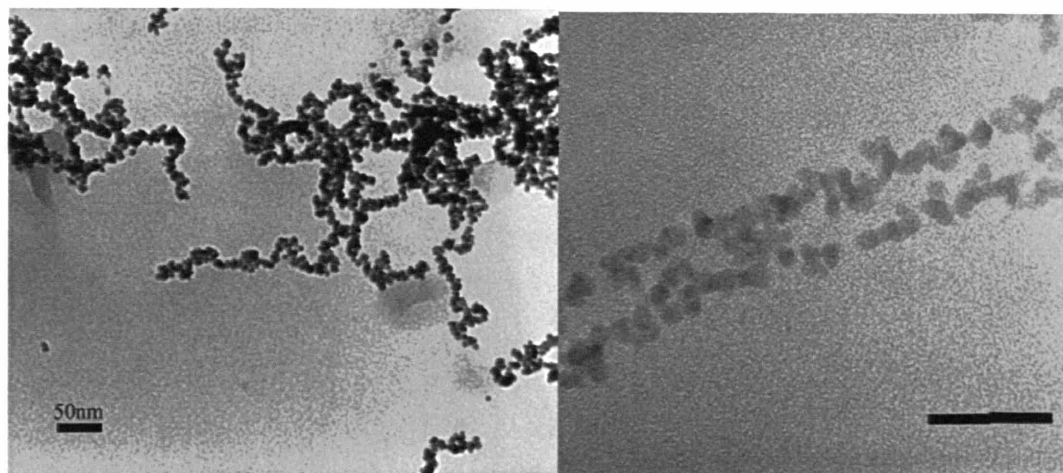

Figure 4.8. Unannealed CoPt nanoparticle-phage assemblies. Scale bars are 50nm and 20nm for the images on the left and right respectively.

Annealing of the CoPt and FePt assemblies at 350° C was necessary for the removal of

the virus template and promoted growth of crystalline nanowires that retained the $L1_0$ phase of

the as-prepared particles and were uniform in diameter (10nm +/- 5%). The crystalline nature of the wires can be seen in the selected area ED pattern (figure 4.8a, insert), which also shows the characteristic (001) and (110) $L1_0$ peaks, and by HRTEM lattice imaging. The (111) plane perpendicular to the long axis of the CoPt wires with a lattice spacing of 2.177 Å was in agreement with the reported value of 2.176 Å, and again confirmed the highly crystalline nature of the material (figure 4.8 b, JCPDS #43-1358). Electron diffraction of the annealed CoPt wires reveals the superlattice structure unique to the $L1_0$ phase (figure 4.8 b, insert). The persistence of the $L1_0$ phase, which has been traditionally accessible only above $550°$ C (26), was attributed to the propensity of particles to maintain their original orientation during aggregation-based annealing.
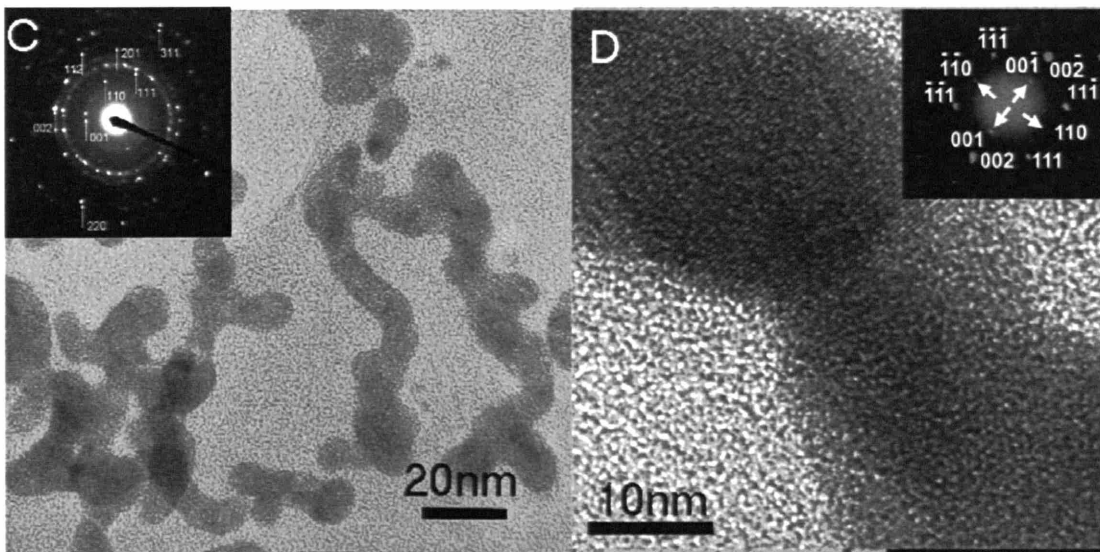
Figure 4.8 Annealed CoPt nanowires. Contious inorganic structures exhibit the characteristic $L1_o$ peaks in the ED pattern (left, insert). HRTEM shows continuation of the crystal direction beyond the grain boundary (right). The superlattice structure of the $L1_0$ phase is evident by the ED pattern (insert).

This synthetic route also proved effective for the FePt system with Electron diffraction of the unannealed FePt wires and annealed FePt wires confirming the $L1_0$ nature of the FePt wires and showing the crystalline nature of the material (figure 4.9).
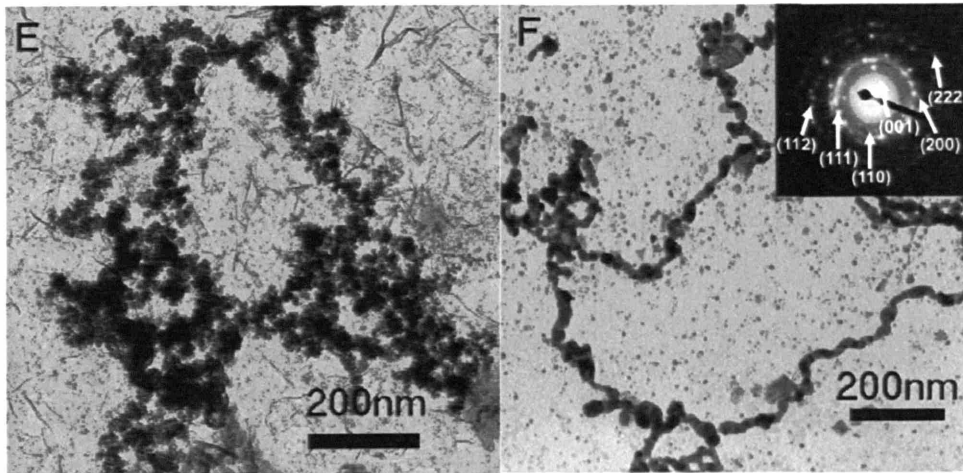
Figure 4.9 FePt nanoparticle-phage assemblies before (left) and after (right annealing). Electron diffraction of the post annealed assemblies (at a 350°C, below the $L1_0$ transition temperature) confirms the presence of the $L1_0$ phase.

Magnetic analysis of the unannealed CoPt nanoparticles showed superparamagnetic behavior, suggesting that even though the presence of the $L1_0$ magnetic phase is present as confirmed by electron diffraction, either the particle size is below the critical limit or that there is a majority formation of non-chemically ordered CoPt particles (figure 4.10). Particles having an effective size below the critical limit is believed to be caused by oxidation, and their intrinsically smaller size compared to the FePt system.
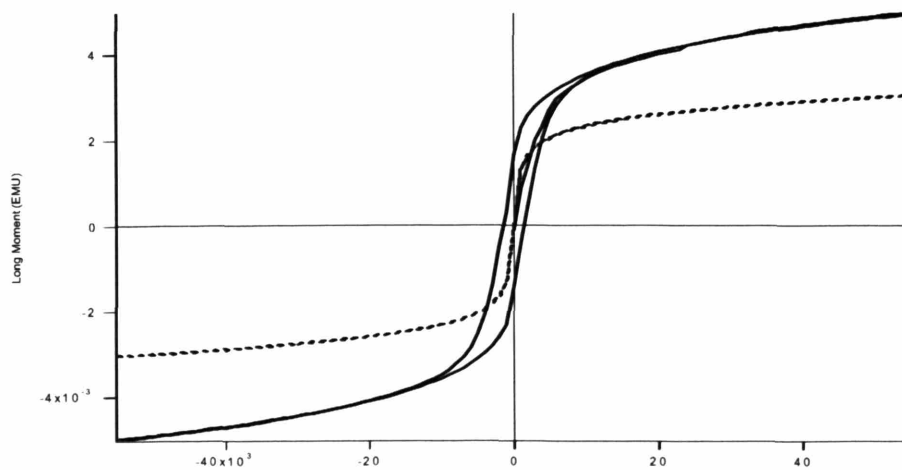
Figure 4.10 SQUID of the CoPt nanoparticles synthesized using the CoPt specific dodecapeptide at 300K (dashed) and 5K (solid).

Thermal gravimetric analysis of the virus-particle system was used to obtain a critical temperature for the synthesis of crystalline nanowires and showed removal of the organic materials by 350°C. Although the analysis was performed under forming gas, there seemed to evidence of continual material loss above 700°C, and is believed to be actual loss of the inorganic material. No known mechanism for this loss is known, but it has been observed in the laboratory of T. Thompson at IBM Almaden and communicated through personal correspondence (figure 4.11).

This agreed well with the minimum temperature observed for the fusion of adjacent particles by TEM with annealing performed in situ using a thermal stage (figure 4.12). Thermal TEM analysis also revealed the importance of the temperature ramp rate. Rapid temperature increases causes the particle assemblies to form large aggregates rather than wires, as the energy shock promotes the lower energy confirmations of the system (figure 4.13).
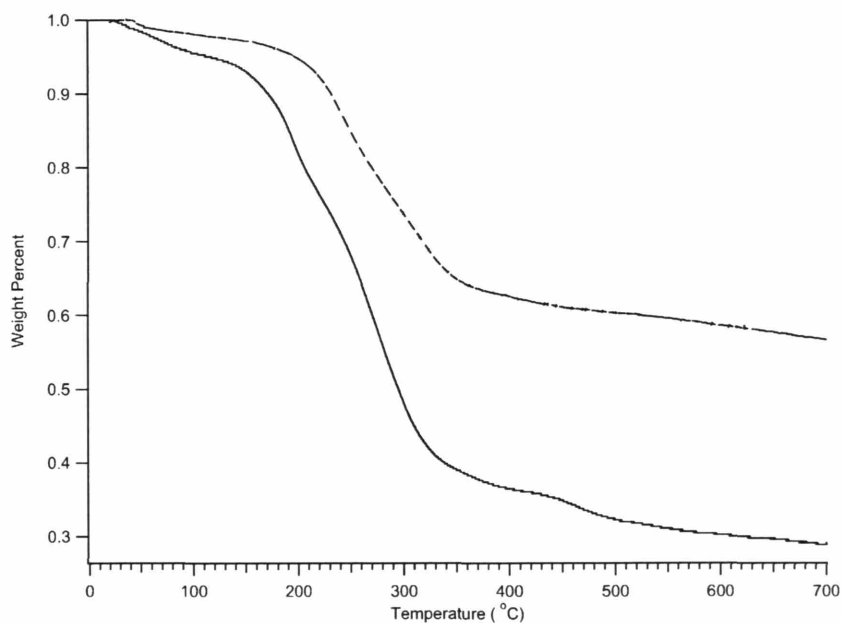
Figure 4.11 TGA analysis of the CoPt nanoparticle-phage assemblies under forming gas (5%H_2, dashed) and Nitrogen (solid). The reducing effect of the forming gas is evident by the lack of an oxide peak around 450°C. Confirmation of the removal of the phage structure through a NaI/ethanol wash is observed by a significant reduction of the lost material for the sample that had been treated to remove the virus from the system (dashed).
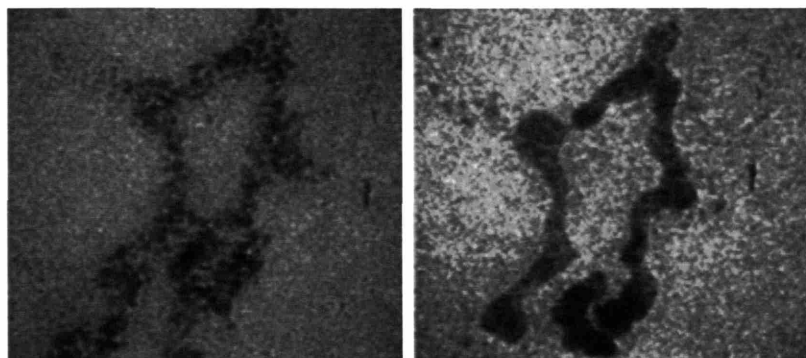

Figure 4.12 in situ thermal anlysis of a CoPT nanoparticle-phage assembly performed in the TEM. Transformation of the nanoparticles into continuos structures occurs at approximately 300° C.
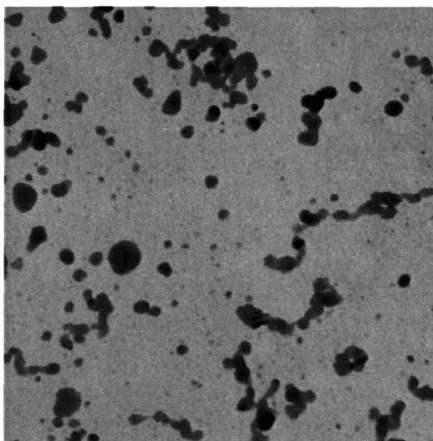
Figure 4.13 TEM micrograph of a CoPt nanoparticle-phage assembly at 400°C.

4.4 *Discussion*

Nature has evolved numerous proteins to control the crystallization of ionic solids, like $CaCO_3$. The ferromagnetic materials synthesized in these experiments are radically different from ionic solids prepared using precipitation reactions. These materials are metallic alloys and are prepared by the reduction of metallic ions. The application of this technology to radically different materials and different chemical reactions suggests that peptides have the potential to fabricate a variety of inorganic materials that are not naturally evolved to coexist with biological systems. However, this control over organization and length scale that biology has fine tuned can be applied to these technologically important materials. This approach to synthesizing inorganic materials is more environmentally friendly because it does not require halogenated organic solvents like the alternative preparations. Additionally, the protocol is very robust and could be applied to alternative magnetic materials.

The exploitation of the self-assembly motifs employed by the M13 bacteriophage to produce a biological scaffold provides a means of generating a complex, highly ordered, and economical template for the general synthesis of single crystal nanowires. By introducing

programmable genetic control over the composition, phase and assembly of nanoparticles, a generic template for the universal synthesis of a variety of materials can be realized. Further advances in the fabrication of nanoscale materials and devices can be achieved through modification of the remaining four proteins in the virus to incorporate device-assembly directors. Overall, modification of biological systems by the introduction of substrate specific peptides presents a means of achieving well ordered nanomaterials in a cost-effective and scalable manner.

References

1.   Mao, C. et al. Viral Assembly of Oriented Quantum Dot Nanowires. *Proc. Nat. Academ. Sci. in press* (2002).

2.   Fowler, C. E., Shenton, W., Stubbs, G. & Mann, S. Tobacco Mosaic Virus Liquid Crystals as Templates for the Interior Design of Silica Mesophases and Nanoparticles. *Adv. Mater.* **13**, 1266-1269 (2001).

3.   Douglas, T. et al. Synthesis and Structure of an Iron (III) Sulfide-Ferritin Bioinorganic Nanocomposite. *Science* **269**, 54-57 (1995).

4.   Wong, K. K. W. & Mann, S. Biomimetric Synthesis of Cadmium Sulfide -Ferritin Nanocomposites. *Adv. Mater.* **8**, 928-933 (1996).

5.   Brown, S., Sarikaya, M. & Johnson, E. A Genetic Analysis of Crystal Growth. *J. Mol. Biol.* **299**, 725-735 (2000).

6.   Mattoussi, H. et. al. Self-assembly of CdSe-ZnS quantum dot bioconjugates using an engineered recombinant protein. *J. Am. Chem. Soc.* **2000**

7.   Falini, G., Albeck, S., Weiner, S. & Addadi, L. Control of Aragonite or Calcite Polymorphism by Mollusk Shell Macromolecules. *Science* **271**, 67-69 (1996).

8.   Reiss, B.D.; Mao, C.; Solis, D.J.; Ryan, K.S.; Thompson, T.; Belcher, A.M. Biological Routes to Metal Alloy Ferromagnetic Nanostructures. *Nano Letters* **2004**, *4*(6), p. 1127-1132.

9.   E. Dujardin *et. al.*, Organization of metallic nanoparticles using tobacco mosaic virus templates. *Nano Lett.* **2003**, *3*, pp. 413-417.

10. Mao, C.;* Solis, D.J.;* Reiss, B.D.; Kottmann, S.T.; Sweeney, R.Y.; Hayhurst, A.; Georgiou, G.; Iverson, B.; Belcher, A.M. Virus-Based Toolkit for the Directed Synthesis of Magnetic and Semiconducting Nanowires. *Science* **2004,** *203*, p. 213-217.

11. Martin, D.A. Filamentous phage structure, infection and assembly. *Curr. Opin. Struct. Bio.* **1998**, *8*, pp. 150-158.

12. J. F. Banfield *et. al.*, *Science* **289**, 751 (2000).

13. Sun, S., Murray, C. B., Weller, D., Folks, L. & Moser, A. Monodisperse FePt nanoparticles and Ferromagnetic FePt Nanocrystal Superlattices. *Science* **287**, 1989-92 (2000).

14. Dai, Z. R., Sun, S. & Wang, Z. L. Phase Transformation, Coalescence, and Twinning of Monodisperse FePt Nanocrystals. *Nanoletters* **1**, 443-447 (2001).

15. Weller, D. & Moser, A. Thermal Effect Limits in Ultrahigh-Density Magnetic Recording. *IEEE Trans. Mag.* **35**, 4423-4439 (1999).

16. Kay, B. K., Winter, J. & McCafferty, J. (eds.) *Phage Display of Peptides and Proteins* (Academic Press, San Diego, 1996).

17. Warne, B., Kasyutich, O. I., Mayes, E. L., Wiggins, J. A. L. & Wong, K. K. W. Self Assembled Nanoparticulate Co:Pt for Data Storage Applications. *IEEE Trans. Mag.* **36**, 3009-3011 (2000).

18. Alivisatos, A.P. Enhanced: Naturally aligned nanocrystals *Science* **289**, 736 (2000).

19. W. D. Luedtke, U. Landman, *J. Phys. Chem.* **100**, 13323 (1996).

20. Qadri,S.B.;, Skelton, E.F., Hsu, D., Dinsmore, A.D., Yang, J. Gray, H.F., Rama, B.R. Size-induced transition-temperature reduction in nanoparticles of ZnS. *Phys. Rev. B* **60**, 9191 (1999).

21. X. Duan, C. M. Lieber, *Adv. Mat.* **12**, 298 (2000).

22. C. Ye, G. Meng, Y. Wang, Z. Jiang, L. Zhang, *J. Phys. Chem. B* **106**, 10338 (2002).

23. R. L. Penn, J. F. Banfield, *Geochimica et Cosmochimica Acta.* **63**, 1549 (1999).

24. S. Sun, C. B. Murray, D. Weller, L. Folks, A. Moser, *Science* **287**, 1989 (2000).

25. Y. H. Huang, H. Okumura, G. C. Hadjipanayis, D. Weller, *J. Appl. Phys.* **91**, 6869 (2002).

26. K. Barmak *et. al.*, *Appl. Phys. Lett.* **80**, 4268 (2002).

5.1 *Introduction*

Development of genetically modified virus-based scaffolds for the patterning and assembly of nanoscaled materials for their incorporation into functional devices relies on every aspect of the previous research (*1,2*). Assembly and nucleation directing peptides, selected through the combinatorial screening process of phage display, that exhibit substrate specificity and control of nanoparticle formation, have been simultaneously expressed on the proximal tip and capsid of the highly ordered filamentous M13 bacteriophage virus. This allows for the directed placement of the virus onto pre-patterned electrodes and the subsequent growth of ordered, liner arrays of nanoparticles of controlled composition, phase and size. Removal of the viral template via thermal annealing leaves purely inorganic nanowires that bridge the electrode gap (figure 5.1). The unique ability to interchange substrate specific peptides into the proximal and remote tips of the filamentous construct of the M13 virus, while controlling materials synthesis along the capsid, provides a unique means of patterning nanostructures for their use in electronic devices.
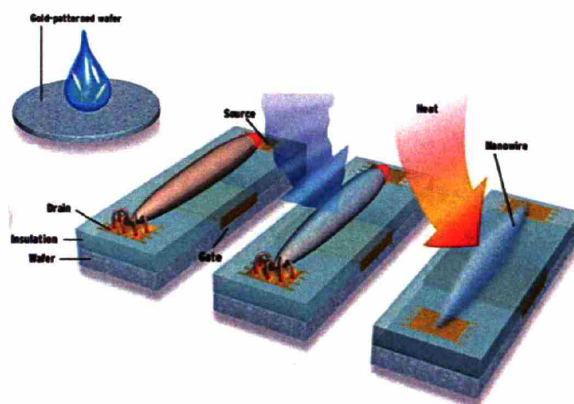

Figure 5.1 Phage directed assembly of nanoscale electronics. . (image from IEEE spectrum, Germs that build circuits, online.)

Physical (*3,4*), chemical (*5,6*) and biological (*7*) strategies have all had success in controlling the physical shape, size, composition and phase of advantageous materials at the nanometer scale. However, the incorporation of these building blocks into functional, multi-component devices has proven to be more difficult. Reliance on methods such as direct contact (e-beam), flow deposition (Lieber), polymer dispersions (Alivisatos, Bawendi/Bulovich) and grafting chemistries (gold thiol/ Merkin, s-oligos/DNA, Israely) do not offer the needed specificity for developing multi-component structures in parallel self-assembly synthesis. The inability to incorporate unique assembly moieties into individual nanocomponents has limited the development of more sophisticated heterostructures. In order to multiplex the self-assembly process a complex, materials specific linking scheme must be developed. Nature provides one of the most diverse assembly schemes, wherein a small basis set of amino acids can be combined in an almost infinite way, which allows multiple processes to occur in parallel. We have previously shown the versatility of biological based systems for processing multiple classes of materials within a single synthetic strategy (science), and have now extended the M13 bacteriophage system to include compound functionalities. Development of a gene-linked scaffold that allows for the synthesis and directed assembly of nanoscale materials and devices presents a new paradigm for the one-pot synthesis of complex, multi-component nanoscale heterostructures.

5.2 *Methods and Materials*

Patterned gold electrodes having a gap spacing of 550nm, less than the length of the modified virus (~600nm, due to encapsulation of a shorter DNA vector), were prepared using standard lithographic techniques and used without further modification. The mask was prepared by benchmark technologies and is shown in figure 5.2.
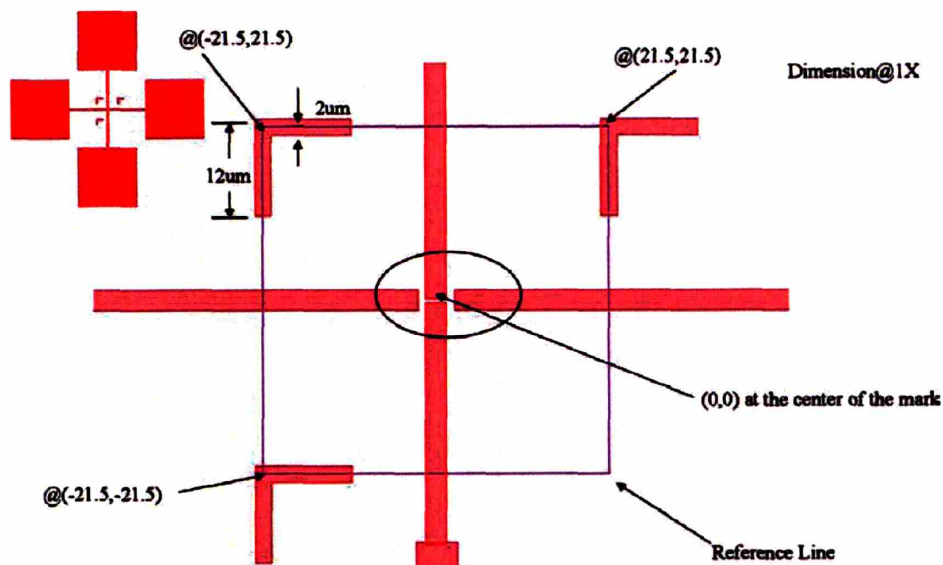
Figure 5.2 Mask of the pre-patterned gold electrodes.

The electrodes where incubated in 1mL of a solution of phage based scaffolds (1x10^12 pfu) that expressed the gold binding motif (LKAHLPPSRLPS) on the proximal tip and the CdS constrained heptapeptide along the capsid for 5-30min, depending on desired surface concentration with constant rocking. After the incubation period the substrate was washed with a directional flow of TBST 1% followed by thorough rinsing with type 1 water, also in a directional flow. The virus bridged electrodes were then dried for imaging by Atomic Force Microscopy (AFM) using compressed nitrogen followed by vacuum desiccation. Images were collected on a Digital Instruments multimode nanoscope IV.

Nucleation of the viruses was achieved by placing the substrate into a 1mM solution of $Cd(NO3)2$ at $0°C$ for 1hour prior to the introduction of HS(g) via a bubbler, and was performed in a hood with a sulfide scrub before and after the reaction vessel (water was used as a scrub before the RV and water plus excess $Cd(NO3)_2$ was used after.) HS gas was chosen to limit the

formation of salt on the substrate. pH effects of the dissolved HS never drop below 4, higher than the elution buffer (pH 2.3), and should therefore not dramatically effect phage binding.

Processed substrates were then annealed to remove the phage template using a Thermolyne tube furnace operating at 300°C under atmospheric conditions. Annealing at temperatures used during the nanowire synthesis reported in chapter 4 causes dewetting of the CdS from the gold and results in large crystallite formation (figure 5.3).
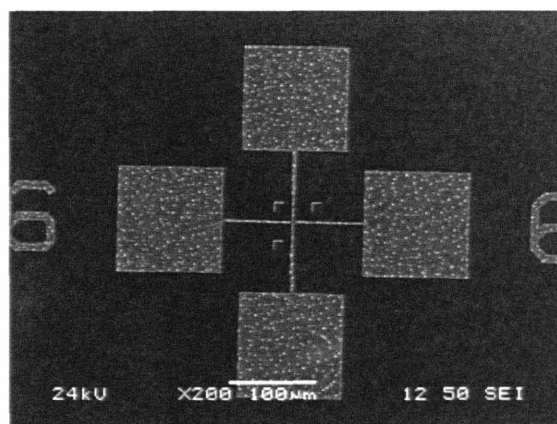
Figure 5.3 CdS aggregation after annealing at 425°C for 1 hour.

Electrical measurements were performed at a probe station using an Agilent 4156c semiconductor parameter analyzer.

5.3 Specific attachment of Bacteriophage

Genetically programmed bacteriophage, designed to locate pre-patterned electrodes and bridge them with functional materials have been prepared using standard biological techniques discussed previously. AFM imaging of substrates incubated with the engineered phage scaffold shows the ability to attach the bacteriophage to pre-patterned electrodes. The evident flaring of the viruses off of the gold electrodes, and lack of viruses elsewhere on the substrate demonstrates the specificity of the virus (figure 5.4).
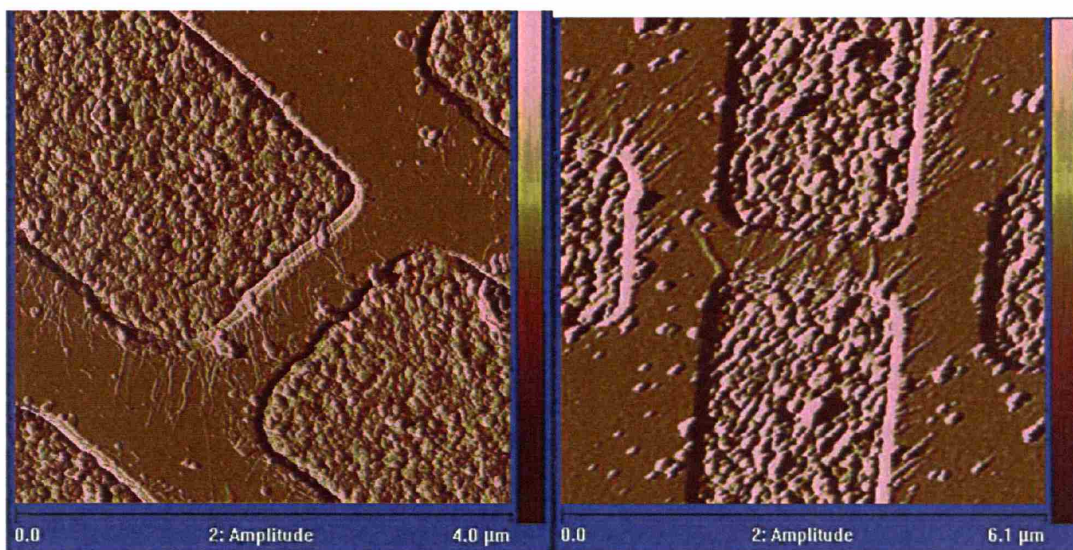
Figure 5.4 AFM Amplitude micrographs of electrode bound phage.

The directionality of the virus also confirms the effectiveness of the flow alignment for bridging the electrode gap. By controlling the deposition conditions (ionic strength, phage concentration) and the wash conditions (wash time, surfactants) the number of phage bridging the gap can be varied from complete coverage to single viruses and is consistent across the wafer (1cm x 1cm) (Figure 5.5 b,c,d).
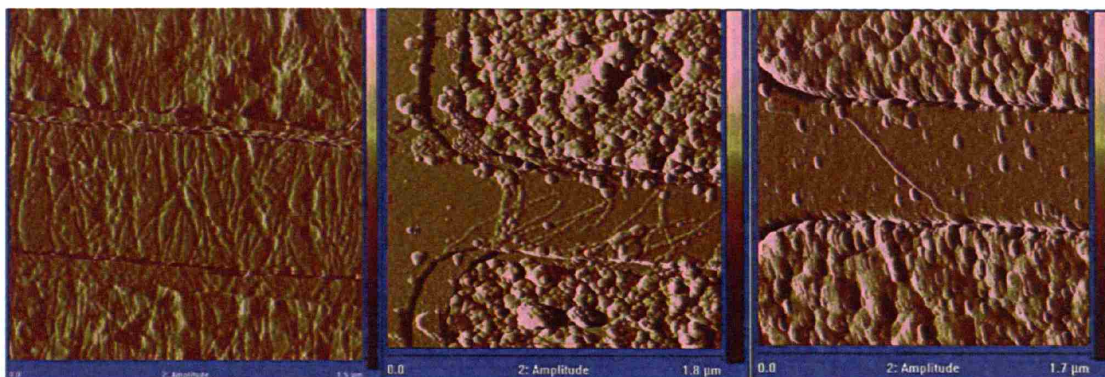

Figure 5.5 Bridging density of the phage is controlled by deposition time and wash conditions.

Incorporation of other binding moieties on the distal tip, or design of a different scaffold can be used to develop more complex devices, but is limited here to simple bridging events as a proof of concept system.

5.4 *Nucleation*

After deposition of the modified virus onto the pre-patterned electrodes, nucleation of materials could take place. CdS specific peptides are utilized in the presented work, but this system can be extended to the previous systems reported (ZnS, CoPt, FePt). Confirmation of nucleation was achieved using AFM and SEM. The localization of the nucleated material to phage rich regions of the substrate both on and surrounding the electrodes confirms the ability of the virus to direct the nucleation of material in a prescribed fashion (figure 5.6).
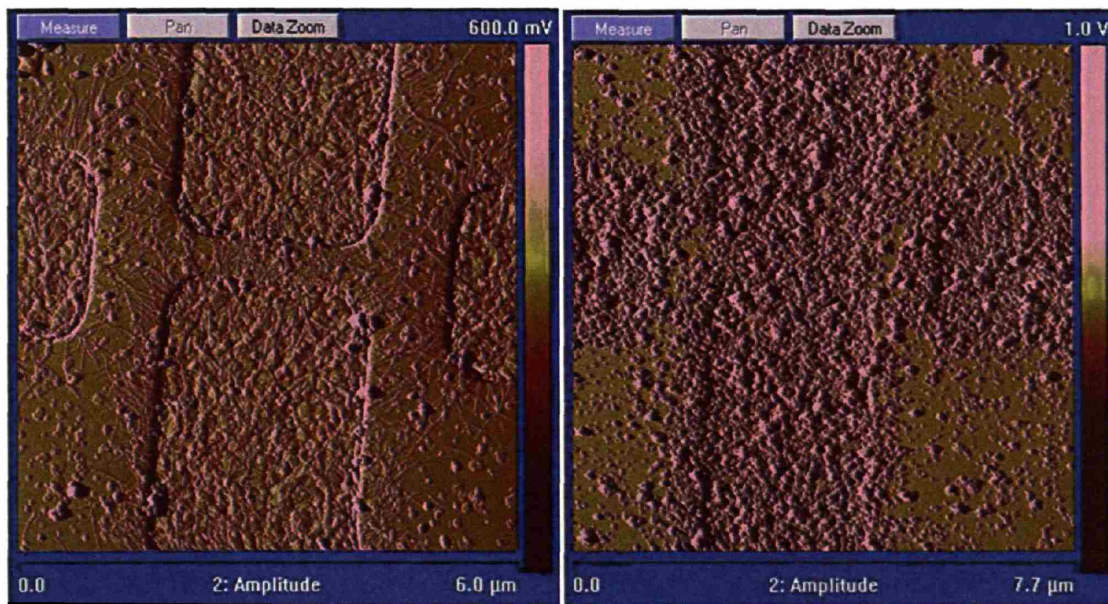

Figure 5.6 Specific binding of the bacteriophage (left) is followed by site specific nucleation of CdS.

Matting of the phage on the electrodes was allowed to develop a large enough bridging density for making reasonable electrical measurements. Mineralization of this phage matt is

shown in figure 5.7. If the phage were not mineralized they would not be visible under the electron microscope. A control in which no phage were added to the process, shows no signs of CdS nucleation.
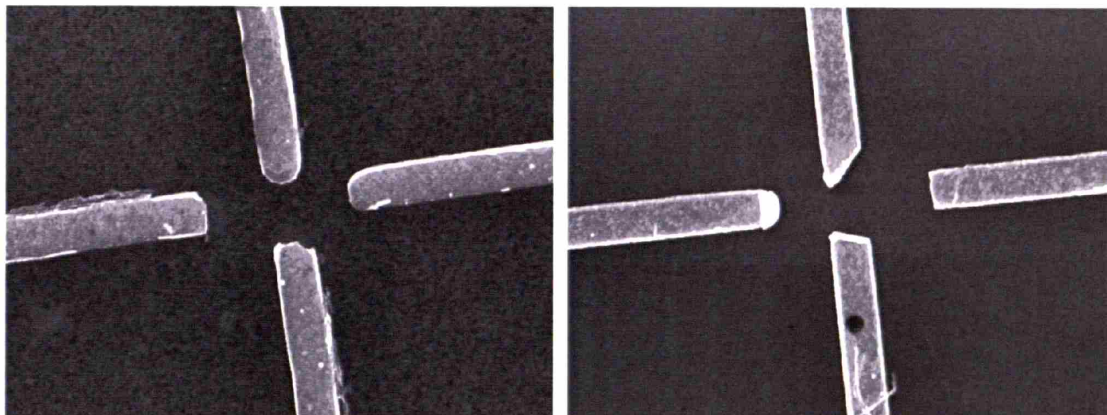

Figure 5.7 Matting of the phage on the electrodes followed by CdS nucleation creats a high bridging density across the electrode gap. As a control, a substrate was processed in a similar manner, with the only exception being the lack of phage.

5.5 *Device Characteristics*

Prior to mineralization, no current is able to pass through the virus bridges (figure 5.8 a). Post nucleation(figure 5.8b), the CdS nanoparticle field present in the electrode gap is able to pass current on the Picoamp scale (figure 5.9).
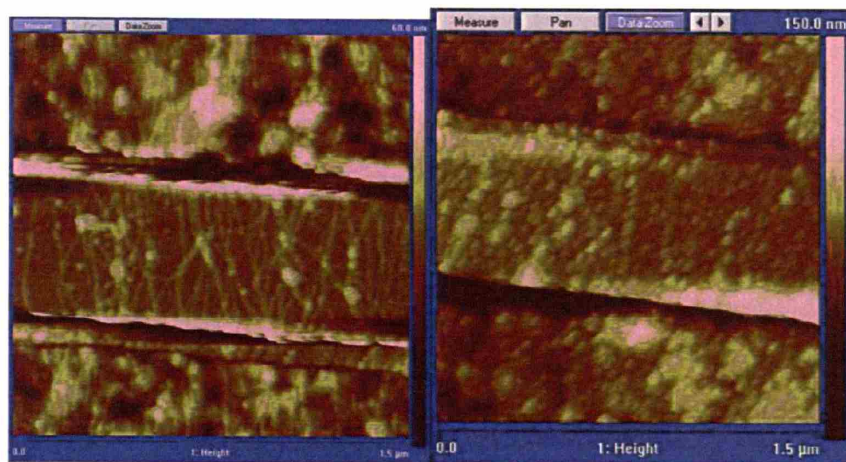

Figure 5.8 AFM height images of pure phage (left) and CdS nucleated phage (right) bridging prepatterned electrodes.

As the particles are not fused and do not form a continuous electrical connection we believe that this current is due to a hopping effect through the particle field as evident by the linear IV curve and the lack of a breakdown current within the 10v range.
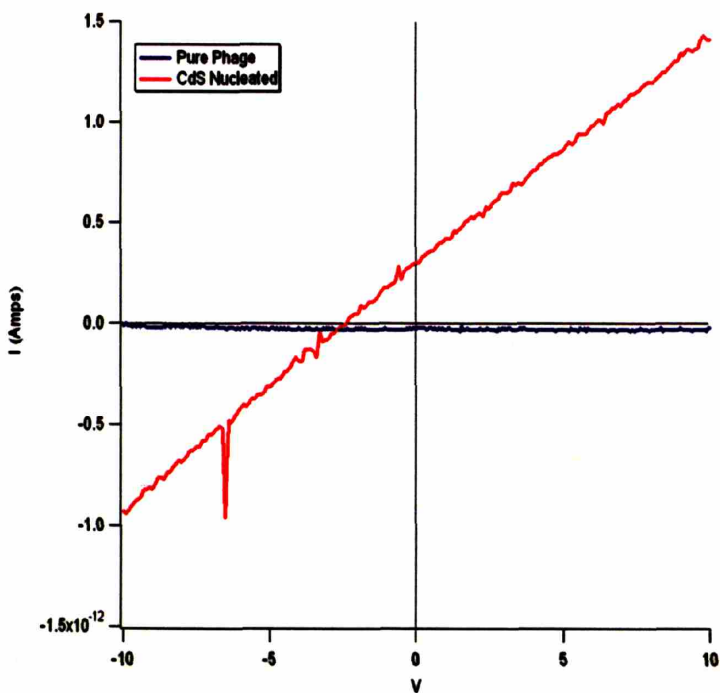

Figure 5.9 IV characteristics of pure phage and as synthesized CdS nanoparticles.

Annealing of the matted phage mineralized with CdS formed large sheets of CdS that dewetted from the gold electrodes. Again, electrodes not exposed to phage prior to interaction with the CdS precursors show no materials growth (figure 5.10).
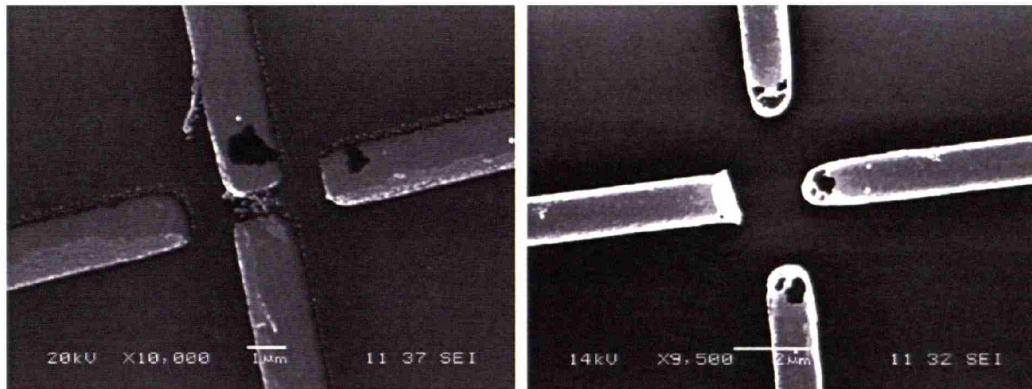
Figure 5.10 SEM micrographs of phage/CdS incubated electrodes after nucleation (left) and a sontrol not incubated with phage.

Initial electrical measurements on the annealed system demonstrate the ability to pass a minimal, but repeatable and realistic current. However, semi-conducting behavior has not been achieved on the current samples, and should be explored further using more in depth probing techniques.
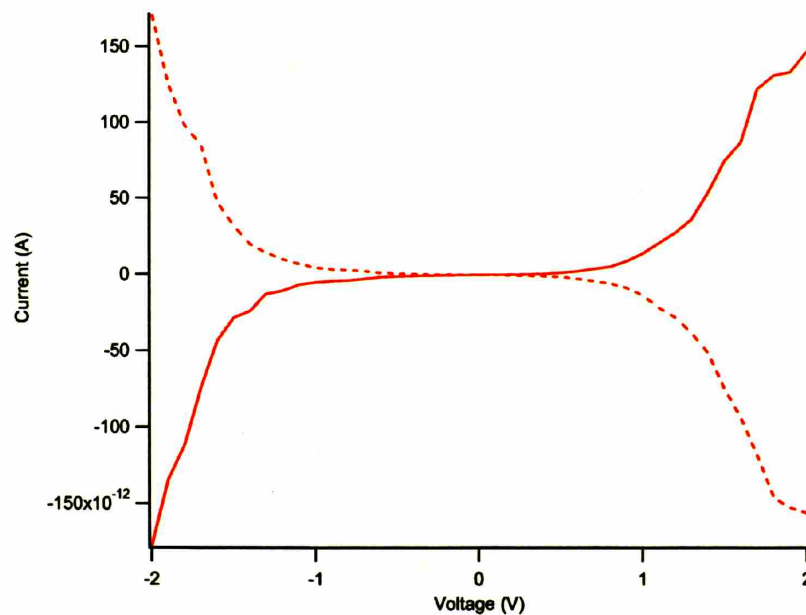

Figure 5.11 IV measurement of CdS mineralized and annealed structures. Both current into (dashed) and out of (solid) the structures is plotted. The passage of 50-150pA of current is expected for the size scale of the structures.

5.6 *Discussion*

A straight forward approach toward introducing multiple assembly moieties within a single scaffold for the synthesis of complex nanoscale devices has been developed. Because of the rapid peptide selection process and ease of genetic modification, the M13 bacteriophage provides a tunable, multifunctional template for the intelligent design of nanoscale devices. The synergy between using the M13 virus as both the screening vehicle and the synthesis scaffold eases the transition between peptide discovery and utilization. It also provides a generic template for designing nano-architectures and gene-linking of that design into the DNA of the virus. The ability to direct the placement and synthesis of CdS nanowires using the M13 bacteriophage in a room temperature, aqueous environment demonstrates the potential of this technique as an environmentally sound, generic solution towards incorporating nanoscale building blocks into future technologies.

1. Mao, C.;* Solis, D.J.;* Reiss, B.D.; Kottmann, S.T.; Sweeney, R.Y.; Hayhurst, A.; Georgiou, G.; Iverson, B.; Belcher, A.M. Virus-Based Toolkit for the Directed Synthesis of Magnetic and Semiconducting Nanowires. *Science* **2004**, *203*, p. 213-217.

2. Reiss, B.D.; Mao, C.; Solis, D.J.; Ryan, K.S.; Thompson, T.; Belcher, A.M. Biological Routes to Metal Alloy Ferromagnetic Nanostructures. *Nano Letters* **2004**, *4*(6), p. 1127-1132.

3. Park, Y.D. et. al. Fabrication of nanometer-sized magnetic structures using e-beam patterned deposition masks. *J. App. Phys.* **1997**, *81*(8), pp. 4717-4719.

4. Huang, Y.H.; Okumura, H,; Hadjipanayis, G.C.; Weller, D. CoPt and FePt nanowires by electrodeposition. *J. App. Phys.* **2002**, *91*(10), pp. 6869-6871.

5. Manna, L.; Scher, E.C.; Alivisatos, A.P. Synthesis of soluable and processable Rod-, Arrow-, Teardrop-, and Tetrapod-Shaped CdSe Nanocrystals. *J. Am. Chem. Soc.* **2000**, *122*, pp. 12700-12706.

6. Murray, C.B.; Norris, D.J.; Bawendi, M.G. Synthesis and characterization of nearly monodisperse CdE (E = S, Se, Te) Semiconductor nanocrystallites. *J. Am. Chem. Soc.* **1993**, *115*, pp. 8706-8715.

7. Klem, M.; Willits, D.; Solis, D.J.; Belcher, A.M.; Young, M.; Douglas, T. Bio-inspired Synthesis of Protein-Encapsulated CoPt Nanoparticles. *Advanced Functional Materials* **2005**, *15*(9), p. 1489-1494.

BIOGRAPHICAL NOTE

Daniel Joseph Solis was born on September 8th, 1978 in Oakland, CA where he lived and attended school until the age of 18. After finishing at Skyline High school, he began his studies in Chemistry and Physics at the California Polytechnic State University in San Luis Obispo California. He graduated with a double major in Chemistry and Physics in 2001. He began his graduate studies in physical chemistry at the University of Texas, Austin during the summer after college under the direction of Angela Belcher. He transferred to the Massachusetts Institute of Technology with Professor Belcher in 2002.